Table 2
Comparison of activities of daily living and quality of life scores between elderly subjects with and without depression

Characteristic	K and S town, Indonesia (2003), mean ± standard deviation		*P*-value	N and V town, Vietnam (2003), mean ± standard deviation		*P*-value	S town, Japan (2002), mean ± standard deviation		*P*-value
	With depression* ($n = 139$) GDS-15 ≥ 6	Without depression† ($n = 272$) GDS-15 ≤ 5		With depression* ($n = 65$) GDS-15 ≥ 6	Without depression† ($n = 314$) GDS-15 ≤ 5		With Depression* ($n = 578$) GDS-15 ≥ 6	Without Depression† ($n = 1327$) GDS-15 ≤ 5	
Age	72.2 ± 8.1	72.7 ± 7.0	NS	71.1 ± 8.5	70.7 ± 7.9	0.7	73.7 ± 6.8	74.1 ± 6.5	0.2
ADL score									
Basic ADL (range 0–21)	19.2 ± 3.2	20.6 ± 1.1	<0.001	19.5 ± 2.6	20.1 ± 1.6	0.007	18.9 ± 4.3	20.6± 1.8	<0.001
Self-maintenance (range 0–5)	2.2 ± 1.5	3.0 ± 1.3	<0.001	0.6 ± 0.5	0.5 ± 0.5	NS	3.7 ± 1.8	4.6 ± 1.0	<0.001
Intellectual activity (range 0–4)	0.5 ± 0.9	1.2 ± 1.5	<0.001	2.2 ± 1.7	2.8 ± 1.6	0.02	2.9 ± 1.3	3.6 ± 0.8	<0.001
Social role (range 0–4)	2.6 ± 1.3	3.3 ± 1.1	<0.001	3.2 ± 1.2	3.7 ± 0.7	<0.001	2.4 ± 1.5	3.4 ± 1.0	<0.001
TMIG index (range 0–13)	5.3 ± 3.0	7.5 ± 3.1	<0.001	8.9 ± 4.1	10.3 ± 3.4	0.003	9.0 ± 4.0	11.6 ± 2.3	<0.001
QOL score (range 0–100)									
Sense of subjective health	38.6 ± 29.7	60.5 ± 23.8	<0.001	38.1 ± 18.1	49.2 ± 17.7	<0.001	51.5 ± 19.0	69.4 ± 17.0	<0.001
Relationship with family	70.4 ± 29.1	85.5 ± 15.8	<0.001	63.0 ± 24.4	78.7 ± 15.6	<0.001	69.3 ± 22.3	84.4 ± 14.9	<0.001
Relationship with friends	71.9 ± 23.5	82.3 ± 18.1	<0.001	73.3 ± 19.0	79.1 ± 16.1	0.01	67.3 ± 20.8	81.9 ± 15.7	<0.001
Financial satisfaction	29.0 ± 22.6	49.8 ± 23.1	<0.001	43.7 ± 15.0	52.7 ± 14.3	<0.001	49.7 ± 25.0	65.7 ± 22.3	<0.001
Subjective happiness	47.5 ± 29.0	75.2 ± 21.6	<0.001	47.2 ± 19.6	61.9 ± 16.4	<0.001	57.0 ± 20.4	77.3 ± 15.5	<0.001

Note: Unpaired *t*-test and chi-square test were used for statistical analysis. Japan—Female: (*) 59.0%, (†) 57.5%; $P = 0.5$. Indonesia—Female: (*) 71.9%, (†) 54.0%; $P < 0.001$. Vietnam—Female: (*) 69.2%, (†) 51.9%; $P = 0.01$. TMIG: Tokyo Metropolitan Institute of Gerontology; ADL: activities of daily living; QOL: quality of life.

prevalence of depression in these countries. Even in the case of screening-based detection, however, depression in the elderly was found to be strongly associated with both lower ADL and lower QOL in three different countries.

In conclusion, about 17.2–33.8% of community-dwelling elderly subjects were found to have screening-based depression in three different Asian countries, and depression was found to be strongly associated with both lower ADL and lower QOL. Primary physicians should pay more attention to depression in community-dwelling elderly populations while considering their strategies for treatment, even in developing countries.

Acknowledgements

We would like to thank the physicians in Bandun Hospital, the students, and the staff of both Bogor Agricultural University and Hanoi Agricultural University for their help and support to the study. In addition, we gratefully acknowledge the support of all the patients, who generously found time to fill in the questionnaire. This study was supported in part by Overseas Scientific Research Grant Nos. 14241005 and 15406031 from the Ministry of Education, Science, Culture and Sports, Japan.

References

Beekman, A.T., Copeland, J.R., Prince, M.J., 1999. Review of community prevalence of depression in later life. Br. J. Psychiatry 174, 307–311.

Cho, M.J., Bae, J.N., Suh, G.H., Hahm, B.J., Kim, J.K., Lee, D.W., Kang, M.H., 1999. Validation of Geriatric Depression Scale, Korean Version (GDS) in the assessment of DSM-III-R major depression. J. Korean Neuropsychiatr. Assoc. 38, 48–63.

Gerety, M.B., Williams Jr., J.W., Mulrow, C.D., Cornell, J.E., Kadri, A.A., Rosenberg, J., Chiodo, L.K., Long, M., 1994. Performance of case-finding tools for depression in the nursing home: influence of clinical and functional characteristics and selection of optimal threshold scores. J. Am. Geriatr. Soc. 42, 1103–1109.

Herrmann, N., Mittmann, N., Silver, I.L., Shulman, K.I., Busto, U.A., Shear, N.H., Naranjo, C.A., 1996. A validation study of The Geriatric Depression Scale short form. Int. J. Geriatr. Psychiatr. 11, 457–460.

Ishizaki, T., Watanabe, S., Suzuki, T., Shibata, H., Haga, H., 2000. Predictors for functional decline among nondisabled older Japanese living in a community during a 3-year follow-up. J. Am. Geriatr. Soc. 48, 1424–1429.

Koyano, W., Shibata, H., Nakazato, K., Haga, H., Suyama, Y., 1991. Measurement of competence: reliability and validity of the TMIG Index of Competence. Arch. Gerontol. Geriatr. 13, 103–116.

Koyano, W., Hashimoto, M., Fukawa, T., Shibata, H., Gunji, A., 1993. Functional capacity of the elderly: measurement by the TMIG Index of Competence. Nippon Koshu Eisei Zasshi 40, 468–474 (in Japanese, Abstract in English).

Lyness, J.M., Noel, T.K., Cox, C., King, D.A., Conwell, Y., Caine, E.D., 1997. Screening for depression in elderly primary care patients. A comparison of the Center for Epidemiologic Studies-Depression Scale and the Geriatric Depression Scale. Arch. Intern. Med. 157, 449–454.

Matsubayashi, K., Okumiya, K., Wada, T., Fujisawa, M., Taoka, H., Kimura, S., Doi, Y., 1994. Comparative study of activity of daily living in the elderly between in Kahoku and in Yaku. Jpn. J. Geriatr. 31, 759–767 (in Japanese, Abstract in English).

Matsubayashi, K., Okumiya, K., Osaki, Y., Fujisawa, M., Doi, Y., 1997. Quality of life of old people living in the community. Lancet 350, 1521–1522.

Morrison, D.P., 1983. The Crichton Visual Analogue Scale for the assessment of behaviour in the elderly. Acta Psychiatr. Scand. 68, 408–413.

Mulrow, C.D., Williams Jr., J.W., Gerety, M.B., Ramirez, G., Montiel, O.M., Kerber, C., 1995. Case-finding instruments for depression in primary care settings. Ann. Intern. Med. 122, 913–921.

Penninx, B.W., Guralnik, J.M., Ferrucci, L., Simonsick, E.M., Deeg, D.J., Wallace, R.B., 1998. Depressive symptoms and physical decline in community-dwelling older persons. J. Am. Med. Assoc. 279, 1720–1726.

Rowe, J.W., Kahn, R.L., 1987. Human aging: usual and successful. Science 237, 143–149.

Saks, K., Tiit, E., Kaarik, E., Jaanson, K., 2002. Depressive symptoms in older Estonians: prevalence and models. J. Am. Geriatr. Soc. 50, 1164–1165.

Schreiner, A.S., Hayakawa, H., Morimoto, T., Kakuma, T., 2003. Screening for late life depression: cut-off scores for the Geriatric Depression Scale and the Cornell Scale for Depression in Dementia among Japanese subjects. Int. J. Geriatr. Psychiatr. 18, 498–505.

Sheikh, J.I., Yesavage, J.A., 1986. Geriatric Depression Scale (GDS); recent evidence and development of a shorter version. In: Brink, T.L. (Ed.), Clinical Gerontology: A Guide to Assessment and Intervention. Haworth Press, New York, pp. 165–173.

Tsai, S.Y., Cheng, C.Y., Hsu, W.M., Su, T.P., Liu, J.H., Chou, P., 2003. Association between visual impairment and depression in the elderly. J. Formos. Med. Assoc. 102, 86–90.

Unutzer, J., Patrick, D.L., Simon, G., Grembowski, D., Walker, E., Rutter, C., Katon, W., 1997. Depressive symptoms and the cost of health services in HMO patients aged 65 years and older. A 4-year prospective study. J. Am. Med. Assoc. 277, 1618–1623.

Whooley, M.A., Avins, A.L., Miranda, J., Browner, W.S., 1997. Case-finding instruments for depression. Two questions are as good as many. J. Gen. Intern. Med. 12, 439–445.

Whooley, M.A., Stone, B., Soghikian, K., 2000. Randomized trial of case-finding for depression in elderly primary care patients. J. Gen. Intern. Med. 15, 293–300.

Xavier, F.M., Ferraza, M.P., Argimon, I., Trentini, C.M., Poyares, D., Bertollucci, P.H., Bisol, L.W., Moriguchi, E.H., 2002. The DSM-IV 'minor depression' disorder in the oldest-old: prevalence rate, sleep patterns, memory function and quality of life in elderly people of Italian descent in Southern Brazil. Int. J. Geriatr. Psychiatr. 17, 107–116.

Yesavage, J.A., 1988. Geriatric Depression Scale. Psychopharmacol. Bull. 24, 709–711.

Yesavage, J.A., Brink, T.L., Rose, T.L., Lum, O., Huang, V., Adey, M., Leirer, V.O., 1982. Development and validation of a geriatric depression screening scale: a preliminary report. J. Psychiatr. Res. 17, 37–49.

Circ J 2005; **69:** 752–755

Sirolimus-Eluting Stent for In-Stent Restenosis of Left Main Coronary Artery in Takayasu Arteritis

Yutaka Furukawa, MD; Toshihiro Tamura, MD; Masanao Toma, MD; Mitsuru Abe, MD; Naritatsu Saito, MD; Natsuhiko Ehara, MD; Ryoji Taniguchi, MD; Yoshihisa Nakagawa, MD; Toru Kita, MD; Takeshi Kimura, MD

A 53-year-old woman with Takayasu arteritis was admitted to hospital because of worsening exertional angina. Coronary angiography revealed 90% ostial stenosis in the left main coronary artery (LMCA), which also involved the bifurcation of the relatively short LMCA. Because the patient refused coronary bypass surgery, she underwent percutaneous coronary intervention (PCI) and the stenosis was successfully dilated. However, the exertional angina recurred a few months later and again after the second PCI. Finally, a sirolimus-eluting stent was deployed in the in-stent restenotic lesion. The patient has been free from angina pectoris for 6 months after the last PCI and follow-up coronary angiography indicated no restenosis in the LMCA. (*Circ J* 2005; **69:** 752–755)

Key Words: Left main coronary artery disease; Restenosis; Sirolimus-eluting stent; Takayasu arteritis

Takayasu arteritis is a form of large vessel vasculitis with an unclear pathogenesis, although autoimmune mechanisms as well as a genetic etiology are possibly involved in its evolution and progression. Because Takayasu arteritis affects the entire aorta and its major branches, it occasionally complicates coronary artery stenoses. Although revascularization therapy is recommended for such patients, obstructive lesions in the subclavian arteries, active inflammation or severe calcification of the aorta often render coronary bypass grafting impossible. In addition, the long-term outcome of percutaneous coronary intervention (PCI) in patients with Takayasu arteritis is largely unknown. We describe a case of Takayasu arteritis with left main coronary artery (LMCA) stenosis that was successfully treated by sirolimus-eluting stent (SES) deployment after repeated in-stent restenosis following bare metal stenting.

Case Report

A 53-year-old woman was admitted to hospital because of worsening exertional angina. At the age of 42 years, she had been diagnosed as having Takayasu arteritis. Magnetic resonance angiography and ^{99m}technetium pulmonary perfusion scintigraphy revealed an occlusion of the left pulmonary artery and multiple mild stenoses in both of the common carotid and subclavian arteries. She had been treated with oral glucocorticoids (prednisolone) and was generally in good condition for the past 11 years until she presented with exertional angina. Angiography in August 2003 revealed severe (90%) ostial stenosis in a short LMCA with involvement of the distal bifurcation (Fig 1A), an intact right coronary artery (Fig 1B) and total occlusion of the left pulmonary artery (Fig 1C). Collateral circulation via the intercostal arteries had developed between the left internal thoracic artery and left pulmonary circulation. Although coronary bypass surgery was recommended as the first therapeutic option, the patient refused open-chest surgery and PCI was then considered as another option. Because the patient developed unstable angina, a bare metal stent (3.0×15 mm ACS RX Multi-Link™, Guidant) was urgently implanted in her LMCA in September 2003; at that time, SES were not available in Japan. The kissing balloon technique was used for stenosis of the bifurcation of the left anterior descending artery (LAD) (4.0×15 mm POWERSAIL, Guidant) and left circumflex artery (LCX) (2.5×20 mm Maverick2, Boston Scientific). The 90% LMCA stenosis was successfully dilated to 0% (Fig 1D) and the angina completely disappeared. The daily dose of oral prednisolone was increased from 12.5 mg to 20 mg because the blood test suggested enhanced activity of the Takayasu arteritis, showing positive C-reactive protein (CRP: 3.6 mg/dl) and an augmented erythrocyte sedimentation rate (48 mm/h). These inflammatory parameters normalized within 1 month. However, 3 months later, the patient was readmitted for recurrence of the angina. She underwent balloon angioplasty using a 4.0×18 mm POWERSAIL (Guidant) for the LMCA and LAD, and 2.5×15 mm Stormer (Medtronic) for the LCX and the restenosed LMCA lesion was successfully treated. Two months after the second PCI, the patient underwent a third PCI for 90% in-stent restenosis in the LMCA because the angina had recurred. Because of the rapid progression of the repeated restenosis accompanied by extension of the stenosis to ostial LAD and LCX, a SES (3.5×23 mm Cypher, Johnson & Johnson) was implanted for the LMCA and LAD in-stent restenosis lesion. The kissing balloon technique was used with a 4.5×20 mm Quantum Maverick (Boston Scientific) for the LMCA and LAD, and 2.75×

(*Received September 6, 2004; accepted October 13, 2004*)
Department of Cardiovascular Medicine, Kyoto University Graduate School of Medicine, Kyoto, Japan
Mailing address: Yutaka Furukawa, MD, Department of Cardiovascular Medicine, Kyoto University Graduate School of Medicine, 54 Kawaharacho, Shogoin, Sakyo-ku, Kyoto 606-8397, Japan. E-mail: yutakaf@kuhp.kyoto-u.ac.jp

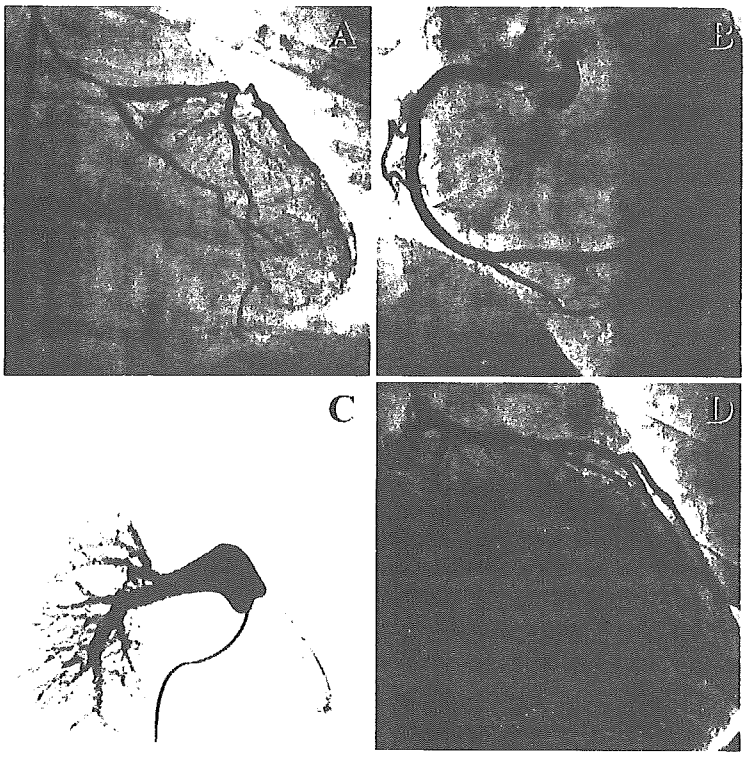

Fig 1. Coronary and pulmonary angiographic findings during the first hospitalization for angina. (A) Left coronary selective injection revealed 90% stenosis in the ostium of the left main coronary artery (LMCA). (B) Intact right coronary artery. (C) Totally occluded left pulmonary artery. (D) Left coronary angiography after percutaneous coronary stenting. The 90% stenosis of the LMCA was successfully dilated to 0%.

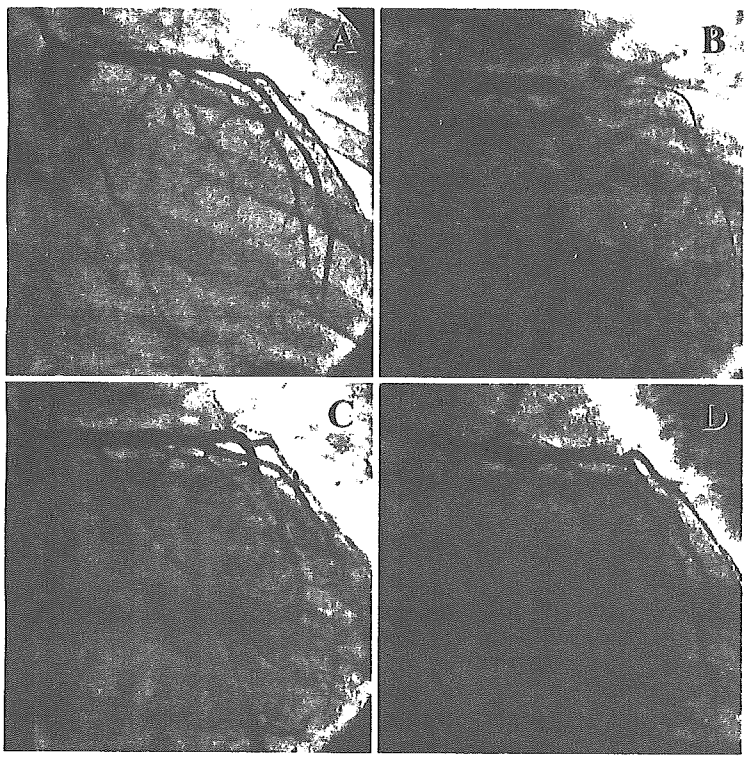

Fig 2. Coronary angiographic findings during the sirolimus-eluting stent implantation (A–C) and at 6-month follow-up. (A) Left coronary angiography shows the 90% in-stent restenosis in the left main coronary artery (LMCA) and ostial left anterior descending artery (LAD). The lesion also involved the ostium of the left circumflex artery (LCX; 90% stenosis). (B) Sirolimus-eluting stent deployed in the LMCA and ostial LAD using the kissing balloon technique (see text for details). (C) The successfully dilated lesion; 0% for the LMCA and LAD, 50% for the LCX. (D) At 6-month follow-up, selective left coronary injection shows no significant restenosis.

20 mm Maverick2 for the LCX (Fig 2A–C).

After the third PCI using the SES, the patient has been free from angina pectoris and follow-up coronary angiography 6 months later showed only minimal luminal narrowing in the LMCA and ostial LCX (Fig 2D).

Discussion

Takayasu arteritis is a large vessel vasculitis that involves the aorta and its main branches, the pulmonary arteries and the coronary arterial tree. However, angina pectoris because of the coronary involvement is not a common feature, having been reported in 6–19% of cases.[1–4] Most of the

coronary stenoses are ostial stenoses of the LMCA and/or right coronary artery[4,5] Coronary revascularization surgery in patients with Takayasu arteritis is often problematic. Stenoses or occlusions of the innominate and subclavian arteries reduce the availability of the internal thoracic arteries as coronary bypass grafts, and active inflammation in the aorta may require an arterial patch with vein grafts at the aortic anastomoses[6] Moreover, Takayasu arteritis is frequently complicated by severe calcification in the aorta, which may also make the bypass surgery arduous[7] For such patients, PCI could be a more beneficial coronary revascularization strategy than coronary bypass grafting.

Recently, PCI has been used as the revascularization therapy for unprotected atherosclerotic LMCA stenosis in poor surgical candidates. Although it has been regarded as contraindicated because of its unacceptably high mortality rate and coronary bypass surgery has been the preferred option[8] advances in techniques and equipment have enabled stenting for unprotected LMCA to be performed with a high initial success rate and acceptable short- to intermediate-term outcome[9] Favorable long-term results of stenting have been also reported in selected patients with normal left ventricular function, although restenosis occurred in approximately 20% of the patients and many of the restenosed lesions required revascularization therapy. In the era of bare metal stenting, restenosis has been the leading cause of major adverse cardiac events after LMCA stenting and has restricted its indication[8] Predictors of refractory restenosis include a short time to restenosis[11] The present case had rapid progression of repeated restenosis and the stenosis extended during each progression. Thus, this is definitely a case of refractory restenosis with a rather poor prognosis. By the time of the third PCI, the distal bifurcation of LMCA was totally involved in the restenotic lesion. PCI for an unprotected LMCA bifurcation lesion is still technically difficult and remains a challenge. Although a variety of strategies have been attempted, residual stenosis in the side-branch ostium and a high rate of restenosis are still common problems[12] In the present case, there was still 50% stenosis of the side branch (LCX) ostium after the third PCI in which a SES was deployed in the parent vessel (LMCA to LAD) and significant late restenosis in the LCX ostium was predicted. However, follow-up angiography at 6 months indicated only minimal additional narrowing of the LCX ostium and 1 possible explanation is the anti-restenotic effects of the eluted sirolimus. Colombo et al have recently reported a lower incidence of restenosis in bifurcation coronary lesions treated with SES and using the kissing balloon technique than in historical bare metal stent controls; nevertheless, restenosis of the side branch remains a problem[13] An aorto-coronary ostial lesion, which was another characteristic of the present case, is also prone to restenosis, but significantly reduced incidence of restenosis after SES deployment has been reported for such lesions[14] Thus, SES shows promise in reducing the rate of restenosis in bifurcation and ostial lesions.

Because most studies of coronary stenting have involved subjects with coronary stenoses of common atherosclerotic etiology, it is uncertain whether coronary stenosis with a prominent inflammatory/immune-mediated etiology such as Takayasu arteritis can be treated as safely and effectively by stenting. Although the results of coronary stenting for Takayasu arteritis have not been reported even in a small group of patients, favorable results of percutaneous stent implantation for aortic as well as major branch stenoses have been indicated[15] In addition, the rate of restenosis after percutaneous transluminal renal angioplasty (PTRA) in chronic stable Takayasu arteritis appears to be lower than for PTRA in common atherosclerotic lesions[16]

The background activity of inflammatory diseases such as Takayasu arteritis may also affects the initial and long-term results of PCI. Arterial stenotic lesions often progress very rapidly in Takayasu arteritis when it is in an active inflammatory phase[17] In the present case, the serum CRP concentration and erythrocyte sedimentation rate were increased at the occurrence of angina, suggesting the recurrence of arterial inflammation caused by the Takayasu arteritis. Although these parameters gradually improved with an increased dosage of prednisolone, enhanced arterial inflammation might have played an important role in the refractory rapid progression of the restenosis after coronary stenting, as well as in the initial onset of angina and its worsening.

Pathological examinations of cases of Takayasu arteritis have shown predominant intimal and adventitial infiltration of T lymphocytes colocalizing with dendritic cells. Dense fibrosis replaces the destroyed medial structure, which normally consists of smooth muscle cells and layered elastic fibers[18] Expression of major histocompatibility complex (MHC)-I, MHC-II and co-stimulatory molecules on the infiltrating cells has also been reported[19,20] These observations suggest that vascular inflammation driven by antigen-specific immune reactions plays a key role in the pathogenesis of the arterial stenoses in Takayasu arteritis and may also facilitate restenosis after coronary stenting. Sirolimus was originally discovered as an antibiotic and then developed as an immunosuppressive agent. It inhibits cell-cycle progression at the late G1 stage and suppresses activated T cell proliferation[21] In addition to its inhibitory effects on T cells, sirolimus markedly suppress the allostimulatory activity of antigen-presenting dendritic cells[22] These immunosuppressive properties of sirolimus may have a beneficial synergistic effect with its anti-proliferative action on vascular smooth muscle cells in the prevention of restenosis after coronary stenting in Takayasu arteritis.

In conclusion, a case of Takayasu arteritis with LMCA in-stent restenosis was successfully treated by a SES. Because of its immunosuppressive effects in the inflamed arterial walls, the SES shows promise for the treatment of stenotic lesions in patients with Takayasu arteritis.

References

1. Koide K. Takayasu arteritis in Japan. *Heart Vessels Suppl* 1992; **7**: 48–54.
2. Hall S, Barr W, Lie JT, Stanson AW, Kazmier FJ, Hunder GG. Takayasu arteritis: A study of 32 North American patients. *Medicine (Baltimore)* 1985; **64**: 89–99.
3. Cipriano PR, Silverman JF, Perlroth MG, Griepp RB, Wexler L. Coronary arterial narrowing in Takayasu's aortitis. *Am J Cardiol* 1977; **39**: 744–750.
4. Endo M, Tomizawa Y, Nishida H, Aomi S, Nakazawa M, Tsurumi Y, et al. Angiographic findings and surgical treatments of coronary artery involvement in Takayasu arteritis. *J Thorac Cardiovasc Surg* 2003; **125**: 570–577.
5. Matsubara O, Kuwata T, Nemoto T, Kasuga T, Numano F. Coronary artery lesions in Takayasu arteritis: Pathological considerations. *Heart Vessels Suppl* 1992; **7**: 26–31.
6. Nakano S, Shimazaki Y, Kaneko M, Taniguchi K, Myamoto Y, Takami H, et al. Transaortic patch angioplasty for left coronary ostial stenosis in a patient with Takayasu's aortitis. *Ann Thorac Surg* 1992; **53**: 694–696.
7. Nishiyama A, Matsubara S, Toyama J. Takayasu arteritis with multi-

ple cardiovascular complications. *Heart Vessels* 2001; **16:** 23–27.
8. Kelley MP, Klugherz BD, Hashemi SM, Meneveau NF, Johnston JM, Matthai WH Jr, et al. One-year clinical outcomes of protected and unprotected left main coronary artery stenting. *Eur Heart J* 2003; **24:** 1554–1559.
9. Black A, Cortina R, Bossi I, Choussat R, Fajadet J, Marco J. Unprotected left main coronary artery stenting: Correlates of midterm survival and impact of patient selection. *J Am Coll Cardiol* 2001; **37:** 832–838.
10. Park SJ, Park SW, Hong MK, Lee CW, Lee JH, Kim JJ, et al. Long-term (three-year) outcomes after stenting of unprotected left main coronary artery stenosis in patients with normal left ventricular function. *Am J Cardiol* 2003; **91:** 12–16.
11. Alfonso F, Cequier A, Zueco J, Moris C, Suarez CP, Colman T, et al. Stenting the stent: Initial results and long-term clinical and angiographic outcome of coronary stenting for patients with in-stent restenosis. *Am J Cardiol* 2000; **85:** 327–332.
12. Sheiban I, Albiero R, Marsico F, Dharmadhikari A, Tzifos V, Pagnotta P, et al. Immediate and long-term results of "T" stenting for bifurcation coronary lesions. *Am J Cardiol* 2000; **85:** 1141–1144, A9.
13. Colombo A, Moses JW, Morice MC, Ludwig J, Holmes DR Jr, Spanos V, et al. Randomized study to evaluate sirolimus-eluting stents implanted at coronary bifurcation lesions. *Circulation* 2004; **109:** 1244–1249.
14. Iakovou I, Ge L, Michev I, Sangiorgi GM, Montorfano M, Airoldi F, et al. Clinical and angiographic outcome after sirolimus-eluting stent implantation in aorto-ostial lesions. *J Am Coll Cardiol* 2004; **44:** 967–971.
15. Nomura M, Kida S, Yamashima T, Yamashita J, Yoshikawa J, Matsui O. Percutaneous transluminal angioplasty and stent placement for subclavian and brachiocephalic artery stenosis in aortitis syndrome. *Cardiovasc Intervent Radiol* 1999; **22:** 427–432.
16. Chatterjee SS, Pahari DK, Sharma RK, Halder B, Roy S, Ghosh S, et al. Long term follow-up of percutaneous transluminal renal angioplasty with special reference to aorto-arteritis. *Indian Heart J* 1995; **47:** 120–124.
17. Numano F, Ohta N, Sasazuki T, HLA and clinical manifestations in Takayasu disease. *Jpn Circ J* 1982; **46:** 184–189.
18. Inder SJ, Bobryshev YV, Cherian SM, Lord RS, Masuda K, Yutani C. Accumulation of lymphocytes, dendritic cells, and granulocytes in the aortic wall affected by Takayasu's disease. *Angiology* 2000; **51:** 565–579.
19. Seko Y. Takayasu arteritis: Insights into immunopathology. *Jpn Heart J* 2000; **41:** 15–26.
20. Seko Y, Sugishita K, Sato O, Takagi A, Tada Y, Matsuo H, et al. Expression of costimulatory molecules (4-1BBL and Fas) and major histocompatibility class I chain-related A (MICA) in aortic tissue with Takayasu's arteritis. *J Vasc Res* 2004; **41:** 84–90.
21. Flanagan WM, Crabtree GR. Rapamycin inhibits p34cdc2 expression and arrests T lymphocyte proliferation at the G1/S transition. *Ann NY Acad Sci* 1993; **696:** 31–37.
22. Chiang PH, Wang L, Bonham CA, Liang X, Fung JJ, Lu L, et al. Mechanistic insights into impaired dendritic cell function by rapamycin: Inhibition of Jak2/Stat4 signaling pathway. *J Immunol* 2004; **172:** 1355–1363.

Effectiveness of Delayed Enhanced MRI for Identification of Cardiac Sarcoidosis: Comparison with Radionuclide Imaging

Eiji Tadamura[1]
Masaki Yamamuro[1]
Shigeto Kubo[1]
Shotaro Kanao[1]
Tsuneo Saga[1]
Masaki Harada[2]
Muneo Ohba[3]
Ryohei Hosokawa[3]
Takeshi Kimura[3]
Toru Kita[3]
Kaori Togashi[1]

OBJECTIVE. The purpose of this study was to evaluate the usefulness of delayed enhanced MRI for detecting cardiac sarcoidosis and to clarify the relationship between the findings of MRI and those of radionuclide imaging.

CONCLUSION. Delayed enhanced MRI is considered a useful method for the early identification of cardiac sarcoidosis. Delayed hyperenhancement is frequently associated with a reduction of regional wall motion and thallium-201 perfusion defects.

Sarcoidosis is a multisystemic disease of unknown cause that is characterized by the formation of noncaseating granulomas [1]. Cardiac sarcoidosis is one of the most important factors determining prognosis [2–4]. Echocardiography, ECG, and radionuclide imaging are commonly used for the diagnosis of cardiac involvement. However, the diagnosis of cardiac involvement is still difficult. It is accurately diagnosed before death in only 29% of patients with fatal cardiac sarcoidosis [5]. Early initiation of corticosteroid therapy in patients with cardiac sarcoidosis improves left ventricular function and prevents malignant arrhythmia [6].

Delayed enhanced MRI was introduced a few years ago to identify myocardial infarctions [7]. This new technique has been shown to detect new or previous myocardial infarction with detail and high spatial resolution [7–10]. This approach also has been used for tissue characterization of various heart diseases [11–15]. However, to our knowledge, no study investigating the usefulness of delayed enhanced MRI for detection of myocardial involvement of sarcoidosis has been published, except for one case report [16]. The purpose of this study was to evaluate the effectiveness of delayed enhanced MRI for detecting cardiac involvement of sarcoidosis and to clarify the relationship between the findings of MRI and those of conventional radionuclide imaging.

Subjects and Methods

Subjects

We studied 10 consecutive patients with cardiac sarcoidosis diagnosed either histologically or clinically according to the following criteria: For the histologic diagnosis group, cardiac sarcoidosis was diagnosed when histologic analysis of operative or endomyocardial biopsy specimens showed epithelioid granuloma without caseating granuloma. For the clinical diagnosis group, consisting of patients with a histologic diagnosis of extracardiac sarcoidosis, cardiac sarcoidosis was diagnosed when complete atrioventricular block, ventricular tachycardia, or emergence of right bundle branch block or premature ventricular contraction (> grade 2 in Lown's classification) was observed. These criteria were modeled on Japanese Ministry of Health and Welfare guidelines for diagnosing cardiac sarcoidosis [17–19]. All patients underwent MRI and scintigraphy using thallium-201 (^{201}Tl) and gallium-67 (^{67}Ga). Coronary angiography was performed on patients with suspected coronary artery disease to exclude coronary artery disease. The protocol was approved by the local institutional ethics committee. Informed consent was obtained from each patient.

MRI

MRI was performed using a 1.5-T whole-body scanner (Symphony, Siemens) with multiple surface coils connected to phased-array receivers. Breath-hold cine MRI was performed using segmented true fast imaging with steady-state precession [20, 21]. The typical imaging parameters were as follows: TR/TE, 3.6/1.8; a 60° flip angle; 13 lines per segment; a 256 × 200 matrix; and a 340 × 320 mm field of view. The temporal resolution was approximately 50 msec. Cine MR images were obtained in the contiguous short-axis planes covering the whole left ventricle [21, 22] and the vertical and horizontal long-axis planes. Fifteen minutes after injection of a

Received August 18, 2004; accepted after revision September 29, 2004.

[1]Department of Nuclear Medicine and Diagnostic Imaging, Kyoto University Graduate School of Medicine, 54 Shogoinkawahara, Sakyo-ku, Kyoto 606-8507, Japan. Address correspondence to E. Tadamura (et@kuhp.kyoto-u.ac.jp).

[2]Department of Endocrinology, Kyoto University Graduate School of Medicine, Kyoto, Japan.

[3]Department of Cardiovascular Medicine, Kyoto University Graduate School of Medicine, Kyoto, Japan.

AJR 2005;185:110–115

0361–803X/05/1851–110

TABLE 1: Patient Profiles and Results of MRI and Scintigraphy

Patient No.	Sex	Age (yr)	Symptom	Involved Organ	ACE (IU/L)	ECG	LVEF (%)	Abnormal Finding in Heart				Entrance Criteria
								Delayed Enhancement	Wall Motion	^{201}Tl	^{67}Ga	
1	M	69	Dyspnea, palpitation	Heart, eye, lung, LN	14.0	RBBB	26	+	+	+	–	Clinical diagnosis
2	F	65	Chest pain	Heart, lung, LN, salivary gland	33.2	RBBB	44	+	+	+	+	Histologic diagnosis
3	F	67	Palpitation	Heart, lung, LN	34.8	RBBB	31	+	+	+	+	Clinical diagnosis
4	F	52	Dyspnea, palpitation	Heart, LN, eye, lung	43.0	Third-degree AVB	65	+	–	–	–	Clinical diagnosis
5	F	77	Syncope	Heart, LN	11.4	Frequent PVC	62	+	–	–	–	Clinical diagnosis
6	M	75	Palpitation	Heart, LN	13.6	Frequent PVC	58	+	+	+	–	Clinical diagnosis
7	M	70	Chest pain	Heart, LN, eye	17.8	Frequent PVC	68	+	–	+	–	Clinical diagnosis
8	F	71	Dyspnea, palpitation	Heart, LN	16.2	RBBB	60	+	–	–	–	Clinical diagnosis
9	F	49	Dyspnea, palpitation	Heart, LN	22.5	Third-degree AVB	54	+	–	–	–	Clinical diagnosis
10	M	35	Dyspnea	Heart, LN, lung	14.2	Frequent PVC	56	+	–	–	–	Clinical diagnosis
Mean		63.0			22.1		52.4					
SD		13.4			11.0		14.2					

Note—ACE = angiotensin-converting enzyme, LVEF = left ventricular ejection fraction, LN = lymph node, RBBB = right bundle branch block, AVB = atrioventricular block, PVC = premature ventricular contractions, plus sign (+) = present, minus sign (–) = absent, ^{201}Tl = thallium-201, ^{67}Ga = gallium-67.

0.15 μmol/kg dose of gadodiamide contrast agent (Omniscan, Nycomed Amersham), delayed enhanced MR images were acquired in the same views as for cine images, using an inversion recovery segmented gradient-echo sequence [7–15]. The typical imaging parameters were as follows: TR/TE, 8.6/3.9; a 25° flip angle, 25 lines per segment, a 256 × 200 matrix, and a 340 × 320 mm field of view. Inversion time (220–360 msec) was optimized for each measurement. In-plane image resolution was typically 1.3 × 1.6 mm. Slice thickness was 8 mm and slice gap was 2 mm.

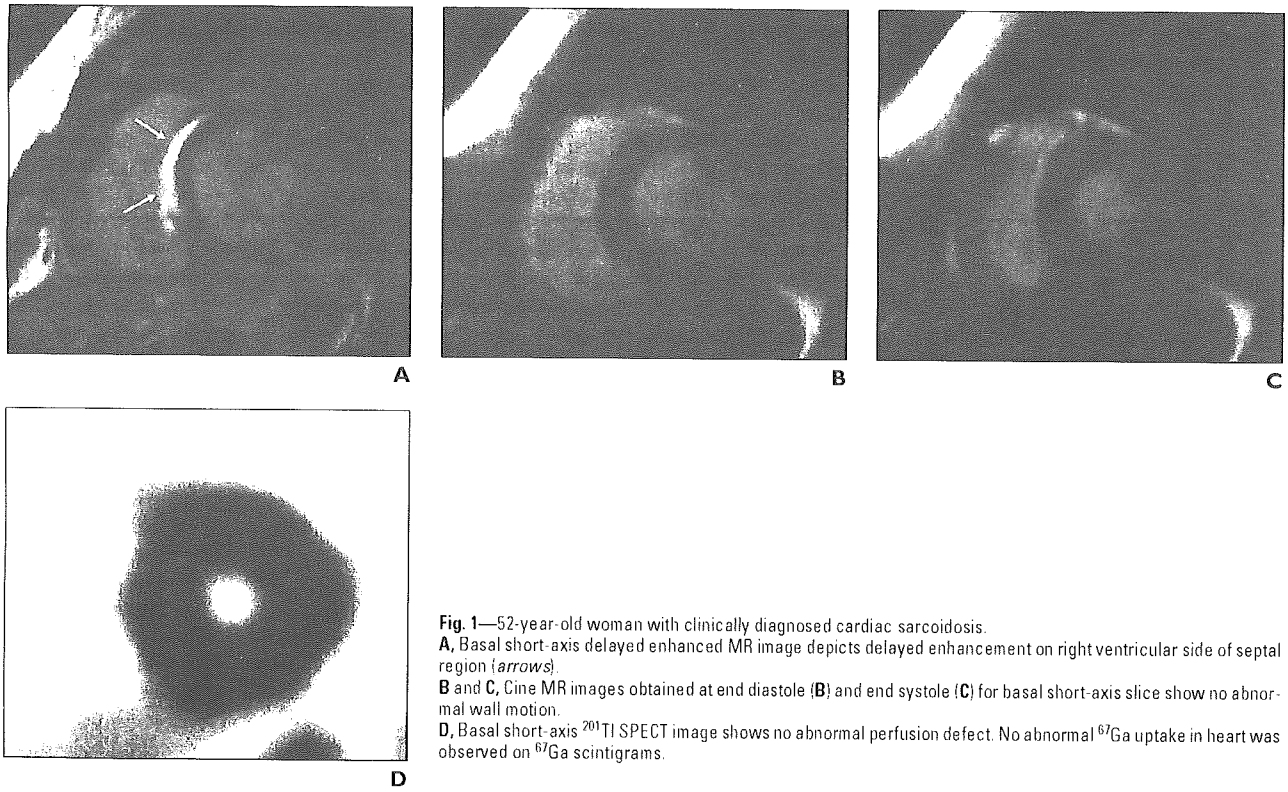

Fig. 1—52-year-old woman with clinically diagnosed cardiac sarcoidosis.
A, Basal short-axis delayed enhanced MR image depicts delayed enhancement on right ventricular side of septal region (*arrows*).
B and **C**, Cine MR images obtained at end diastole (**B**) and end systole (**C**) for basal short-axis slice show no abnormal wall motion.
D, Basal short-axis ^{201}Tl SPECT image shows no abnormal perfusion defect. No abnormal ^{67}Ga uptake in heart was observed on ^{67}Ga scintigrams.

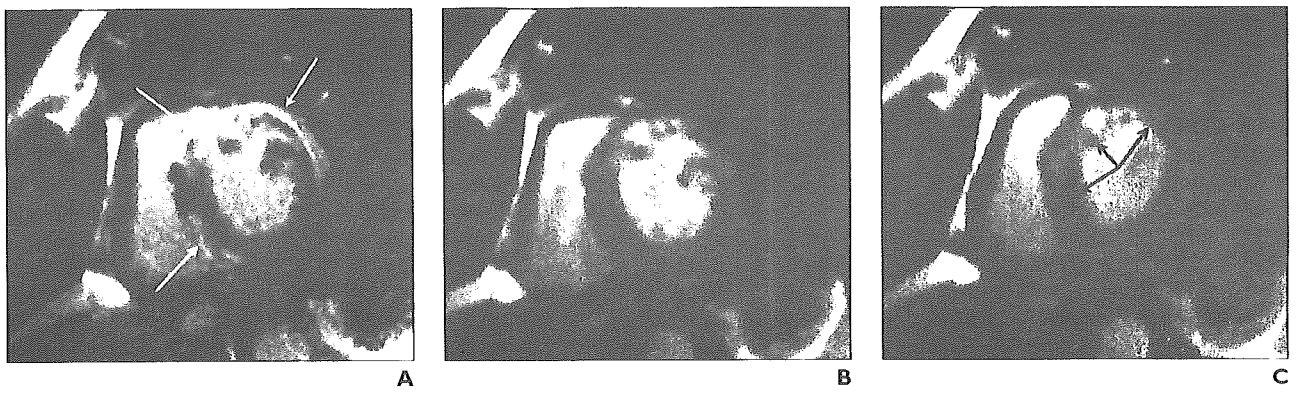

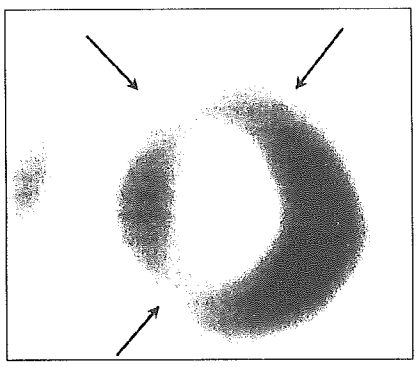

Fig. 2—69-year-old man with clinically diagnosed cardiac sarcoidosis.
A, Basal short-axis delayed enhanced MR image reveals strong transmural hyperenhancement in septal, anterior, and inferior regions (*arrows*).
B and **C,** Cine MR images obtained at end diastole (**B**) and end systole (**C**) for basal short-axis slice show wall motion abnormalities in these segments (*arrows*, **C**).
D, Basal short-axis ^{201}Tl SPECT image shows perfusion defects in septal, anterior, and inferior regions (*arrows*), where severe extent of transmural enhancement is seen on delayed enhanced MR images. No abnormal cardiac ^{67}Ga uptake was detected on ^{67}Ga scintigrams.

Scintigraphic Examinations

^{201}Tl scintigraphy—^{201}Tl (74 MBq) was administered IV under resting conditions. SPECT images were acquired 15 min after injection using a dual-head gamma camera (Millennium, GE Healthcare) equipped with a general-purpose collimator (30 projections over 180°, 30 sec per projection). Two 30% energy windows were used, one centered on the 70-keV peak and one on the 167-keV peak [22, 23].

^{67}Ga scintigraphy—Forty-eight hours after injection of 111 MBq of ^{67}Ga, scintigraphic planar images were acquired using the dual-head gamma camera with medium-energy parallel collimators. Acquisition was performed using three photopeaks (93, 184, and 296 keV) with a 20% window. Thoracic ^{67}Ga SPECT acquisition included three photopeaks, 32 projections over a 360° rotation, and 35 sec per step.

Image Analysis

Left ventricular function was assessed using cine MR images with the aid of commercially available software (Argus, Siemens Medical Solutions) followed by manual corrections of the left ventricular border [21]. Regional analysis of MR images and radionuclide images was performed using the 17-segment model [24]. The average segmental transmural extent of enhancement on delayed enhanced MR images was graded visually by two masked observers using the following scale: 0, no enhancement; 1, 1–25% enhancement; 2, 26–50% enhancement; 3, 51–75% enhancement; and 4, 76–100% enhancement [9]. Segmental wall motion was visually scored as 0, normal; 1, moderate hypokinesis; 2, severe hypokinesis; 3, akinesis; and 4, dyskinesis [9] by two masked investigators. The ^{201}Tl perfusion defect was visually scored by two masked experienced nuclear cardiologists on the basis of severity of reduction in ^{201}Tl activity as 0, normal; 1, mild; 2, moderate; and 3, severe [24]. Two experienced nuclear radiologists visually interpreted ^{67}Ga accumulation while unaware of other results. Consensus was then reached for each visual analysis.

Statistical Analysis

Data are expressed as mean ± SD. Frequency analysis was performed with the Fisher exact test. The mean wall motion score and ^{201}Tl defect score in each hyperenhancement grade were compared using the Mann-Whitney *U* test. A p value of less than 0.05 was considered significant.

Results

Table 1 summarizes the patients' profiles and the results of MRI and radionuclide imaging.

Frequency of Abnormality

Among 10 subjects, five exhibited abnormal delayed enhancement without an abnormality in wall motion or abnormalities shown by radionuclide imaging (Fig. 1). One subject exhibited abnormal delayed enhancement and a ^{201}Tl perfusion defect without regional wall motion abnormalities or abnormal cardiac ^{67}Ga uptake. Two subjects exhibited abnormal delayed enhancement, ^{201}Tl perfusion defects, and regional wall motion abnormalities without cardiac ^{67}Ga accumulation (Fig. 2). Two subjects showed abnormal delayed enhancement, thallium perfusion defects, regional wall motion abnormalities, and abnormal cardiac ^{67}Ga uptake (Fig. 3). Thus, delayed enhancement was observed in every patient with cardiac sarcoidosis (100%). Wall motion abnormalities were observed in four of 10 patients (40%). ^{201}Tl perfusion defects were noted in five subjects (50%). Two patients exhibited abnormal ^{67}Ga accumulation in the heart (20%). Abnormal delayed enhancement was more frequently observed than were ^{201}Tl perfusion defects

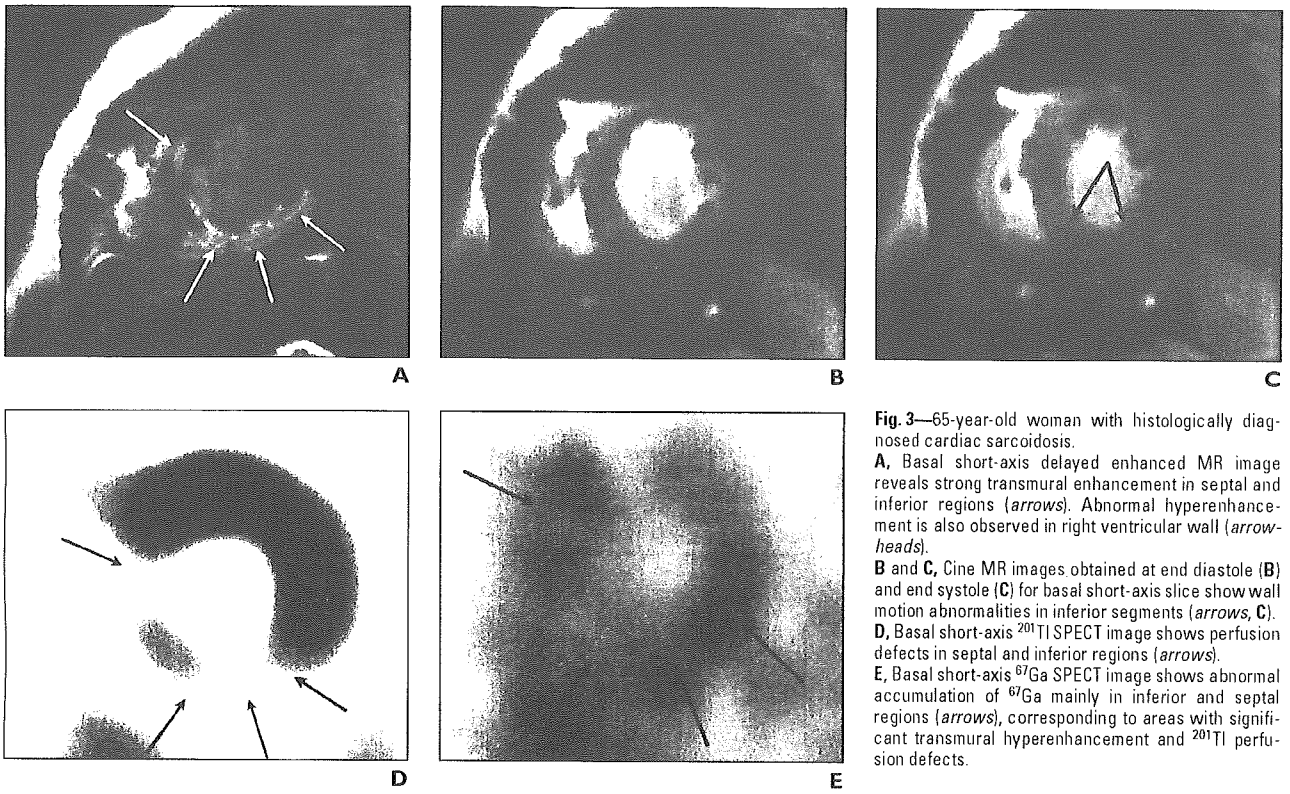

Fig. 3—65-year-old woman with histologically diagnosed cardiac sarcoidosis.
A, Basal short-axis delayed enhanced MR image reveals strong transmural enhancement in septal and inferior regions (*arrows*). Abnormal hyperenhancement is also observed in right ventricular wall (*arrowheads*).
B and **C,** Cine MR images obtained at end diastole (**B**) and end systole (**C**) for basal short-axis slice show wall motion abnormalities in inferior segments (*arrows*, **C**).
D, Basal short-axis ^{201}Tl SPECT image shows perfusion defects in septal and inferior regions (*arrows*).
E, Basal short-axis ^{67}Ga SPECT image shows abnormal accumulation of ^{67}Ga mainly in inferior and septal regions (*arrows*), corresponding to areas with significant transmural hyperenhancement and ^{201}Tl perfusion defects.

($p < 0.05$) or abnormal ^{67}Ga accumulation in the heart ($p < 0.001$).

Location of Abnormal Enhancement

Among the 170 myocardial segments, abnormal delayed enhancement was observed in 48. Figure 4 shows the number of regional segments with abnormal delayed enhancement in the 10 patients. In nine (90%) of the 10 patients, hyperenhancement occurred in the basal septal wall, especially on the right ventricular side (Figs. 1A, 2A, and 3A). The subendocardium of the left ventricle was not involved in seven patients (Fig. 1A).

Wall Motion Abnormality, ^{201}Tl Perfusion Defects, and ^{67}Ga Accumulation Versus Delayed Enhancement

The transmural extent of enhancement on contrast-enhanced MR images correlated significantly with regional ^{201}Tl uptake (Fig. 5) and with regional wall motion (Fig. 6). ^{201}Tl perfusion abnormalities and wall motion abnormalities corresponded to the area showing significant transmural enhancement (Figs. 2 and 3). However, ^{201}Tl perfusion defects or wall motion abnormalities were undetectable in some segments with mild-to-moderate transmural enhancement (Fig. 1). When observed in the heart, abnormal ^{67}Ga accumulation was seen in the segments with severe transmural enhancement and with ^{201}Tl perfusion defects (Fig. 3). On the other hand, delayed enhancement was also observed in regions showing ^{201}Tl perfusion defects without significant ^{67}Ga uptake (Fig. 2).

Discussion

MRI and radionuclide imaging showed a variety of patterns of abnormalities in patients with cardiac sarcoidosis. Among the various findings in MRI and radionuclide imaging, delayed enhanced MRI was considered the most sensitive marker of cardiac involvement of sarcoidosis.

Endomyocardial biopsy may be essential for establishing the diagnosis of cardiac sarcoidosis. However, myocardial biopsies are invasive and, because they are performed blindly and myocardial involvement is not homogeneous, may be insensitive. Echocardiography can detect features such as wall thinning, abnormalities in left ventricular regional wall motion, and pericardial effusion in advanced cardiac sarcoidosis [25–28]. However, early diagnosis of cardiac involvement is difficult on echocardiography. Radionuclide imaging, although it can be helpful for the diagnosis [29–31], does not provide adequate spatial resolution. Indeed, half the cases of cardiac sarcoidosis did not show ^{201}Tl perfusion defects in the current study. MRI has been used to detect cardiac involvement of sarcoidosis [17, 32]. However, those studies used the standard T1-weighted contrast-enhanced spin-echo sequence in which images are acquired without breath-holding. This conventional sequence needs a relatively long acquisition time, which frequently produces respiration motion artifacts [33]. In addition, the contrast between normal and diseased myocardium is not always sufficient [33]. Therefore, we have used a new technique [7–16, 33] for the identification of cardiac involvement of sarcoidosis.

In the current study, delayed enhancement was not always associated with ^{201}Tl perfusion defects or with abnormal ^{67}Ga accumulation. This imperfect association may be caused partly by the poor spatial resolution of radionuclide imaging. However, the transmural extent of hyperenhancement on delayed enhanced MR images correlated significantly with regional ^{201}Tl uptake (Fig. 5). ^{201}Tl perfusion defects were seen in

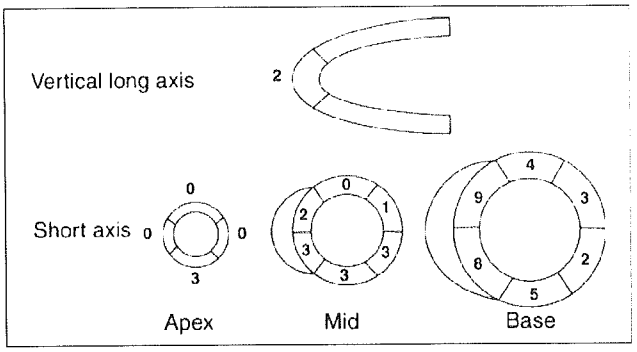

Fig. 4—Number of segments with abnormal delayed enhancement among 17 myocardial segments in 10 patients. Abnormal delayed enhancement was frequently observed in basal septal region.

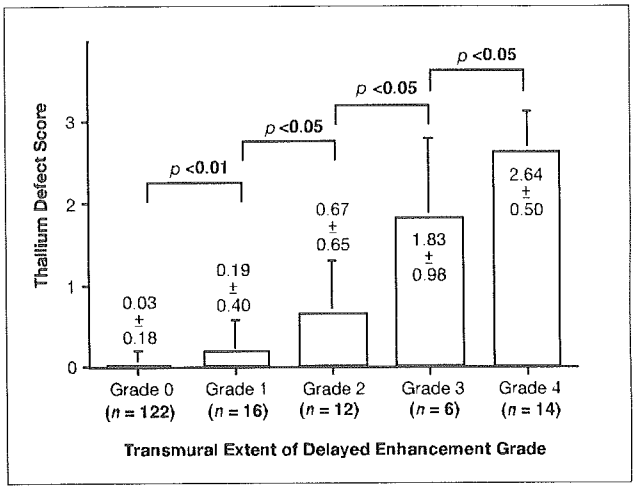

Fig. 5—Bar graph shows relationship between transmural extent of delayed gadolinium enhancement and ^{201}Tl perfusion defects. Significant differences were observed in mean percentage of ^{201}Tl perfusion defect score between segments of grades 0 and 1, grades 1 and 2, grades 2 and 3, and grades 3 and 4.

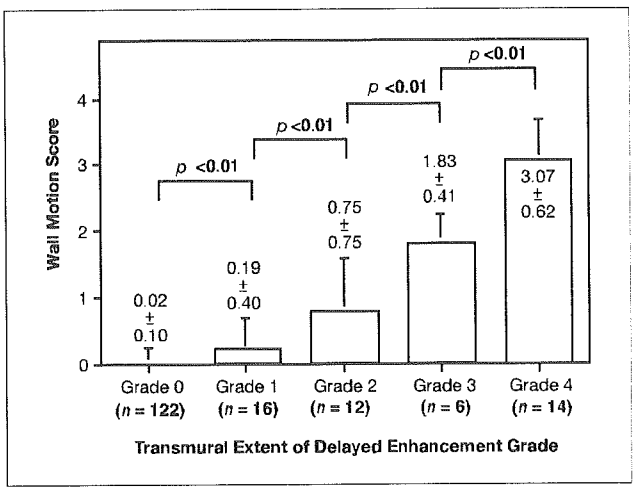

Fig. 6—Bar graph indicates relationship between transmural extent of delayed gadolinium enhancement and regional wall motion. Significant differences were noted in mean percentage of wall motion score between segments of grades 0 and 1, grades 1 and 2, grades 2 and 3, and grades 3 and 4.

the segments with significant transmural delayed enhancement (Figs. 2 and 3). Decreased ^{201}Tl uptake of the myocardium in patients with cardiac sarcoidosis is known to represent fibrogranulomatous replacement of the myocardium [1, 31]. ^{67}Ga scintigraphy has been used to diagnose and evaluate disease activity. In particular, ^{67}Ga accumulation is interpreted as evidence of active inflammatory disease [31]. When abnormal ^{67}Ga accumulation was detected in the heart, the segments with ^{67}Ga uptake corresponded to the areas with considerable transmural delayed enhancement and with ^{201}Tl perfusion defects (Fig. 3). In addition, the transmural extent of hyperenhancement on delayed enhanced MR images significantly correlated with regional wall motion as shown in Figure 6. These findings suggest that the area with delayed enhancement represents myocardium that has been replaced by the fibrogranulomatous tissue of sarcoidosis, resulting in decreased wall motion. On the other hand, regions with ^{201}Tl perfusion defects and no significant ^{67}Ga uptake also showed delayed enhancement (Fig. 2), suggesting that it does not reflect disease activity, although poor spatial resolution might be responsible for undetectable ^{67}Ga uptake.

As shown in Figure 4, delayed enhancement was frequently observed in the basal septal region. This finding is consistent with the findings of previous pathologic and morphologic studies [3, 19, 34, 35] indicating that cardiac involvement of sarcoidosis is common in the basal septal region. The subendocardium of the left ventricle was not involved in seven patients (Fig. 1), unlike the patients with coronary artery disease. Delayed enhancement on the right ventricular side of the basal septal wall might be specific for cardiac involvement in patients with sarcoidosis, because hyperenhancement in this location is uncommon in other cardiac diseases [8, 9, 11, 12, 14]. In addition, this bundle and the right bundle branch are located around this position, possibly accounting for the fact that atrioventricular block or right

bundle branch block is frequently observed in cardiac sarcoidosis.

The major limitation of our study was that cardiac sarcoidosis was proven histologically in only one patient. To confirm our results, further studies should be performed on a large population of patients with histologically proven cardiac sarcoidosis.

In conclusion, delayed enhanced MRI is considered useful for the early identification of cardiac involvement of sarcoidosis. Delayed enhancement is frequently associated with a reduction of regional wall motion and thallium perfusion defects.

References

1. Newman LS, Rose CS, Maier LA. Sarcoidosis. *N Engl J Med* 1997; 336:1224–1234
2. Silverman KJ, Hutchins GM, Bulkley BH. Cardiac sarcoidosis: a clinicopathologic study of 84 unselected patients with systemic sarcoidosis. *Circulation* 1978; 58:1204–1211
3. Matsui Y, Iwai K, Tachibana T, et al. Clinicopathological study on fatal myocardial sarcoidosis. *Ann N Y Acad Sci* 1976; 278:455–469
4. Roberts WC, McAllister HA Jr, Ferrans VJ. Sarcoidosis of the heart: a clinicopathologic study of 35 necropsy patients and review of 78 previously described necropsy patients. *Am J Med* 1977; 63:86–108
5. Perry A, Vuitch F. Causes of death in patients with sarcoidosis: a morphologic study of 38 autopsies with clinicopathologic correlations. *Arch Pathol Lab Med* 1995; 119:167–172
6. Sharma OP. Cardiac and neurologic dysfunction in sarcoidosis. *Clin Chest Med* 1997; 18:813–825
7. Kim RJ, Fieno DS, Parrish TB, et al. Relationship of MRI delayed contrast enhancement to irreversible injury, infarct age, and contractile function. *Circulation* 1999; 100:1992–2002
8. Kim RJ, Wu E, Rafael A, et al. The use of contrast-enhanced magnetic resonance imaging to identify reversible myocardial dysfunction. *N Engl J Med* 2000; 343:1445–1453
9. Wu E, Judd RM, Vargas JD, Klocke FJ, Bonow RO, Kim RJ. Visualisation of presence, location, and transmural extent of healed Q-wave and non-Q-wave myocardial infarction. *Lancet* 2001; 357:21–28
10. Steuer J, Bjerner T, Duvernoy O, et al. Visualisation and quantification of peri-operative myocardial infarction after coronary artery bypass surgery with contrast-enhanced magnetic resonance imaging. *Eur Heart J* 2004; 25:1293–1299
11. McCrohon JA, Moon JC, Prasad SK, et al. Differentiation of heart failure related to dilated cardiomyopathy and coronary artery disease using gadolinium-enhanced cardiovascular magnetic resonance. *Circulation* 2003; 108:54–59
12. Moon JC, Sachdev B, Elkington AG, et al. Gadolinium enhanced cardiovascular magnetic resonance in Anderson-Fabry disease: evidence for a disease specific abnormality of the myocardial interstitium. *Eur Heart J* 2003; 24:2151–2155
13. Bogaert J, Taylor AM, Van Kerkhove F, Dymarkowski S. Use of inversion recovery contrast-enhanced MRI for cardiac imaging: spectrum of applications. *AJR* 2004; 182:609–615
14. Moon JC, Reed E, Sheppard MN, et al. The histologic basis of late gadolinium enhancement cardiovascular magnetic resonance in hypertrophic cardiomyopathy. *J Am Coll Cardiol* 2004; 43:2260–2264
15. Kubo S, Tadamura E, Yamamuro M, et al. Primary cardiac lymphoma demonstrated by delayed contrast-enhanced magnetic resonance imaging. *J Comput Assist Tomogr* 2004; 28:849–851
16. Serra JJ, Monte GU, Mello ES, et al. Cardiac sarcoidosis evaluated by delayed-enhanced magnetic resonance imaging. *Circulation* 2003; 107:e188–e189
17. Shimada T, Shimada K, Sakane T, et al. Diagnosis of cardiac sarcoidosis and evaluation of the effects of steroid therapy by gadolinium-DTPA-enhanced magnetic resonance imaging. *Am J Med* 2001; 110:520–527
18. Yazaki Y, Isobe M, Hiroe M, et al. Prognostic determinants of long-term survival in Japanese patients with cardiac sarcoidosis treated with prednisone. *Am J Cardiol* 2001; 88:1006–1010
19. Yamagishi H, Shirai N, Takagi M, et al. Identification of cardiac sarcoidosis with ^{13}N-NH$_3$/^{18}F-FDG PET. *J Nucl Med* 2003; 44:1030–1036
20. Carr JC, Simonetti O, Bundy J, Li D, Pereles S, Finn JP. Cine MR angiography of the heart with segmented true fast imaging with steady-state precession. *Radiology* 2001; 219:828–834
21. Yamamuro M, Tadamura E, Kubo S, et al. Cardiac functional analysis by multi-detector row CT and segmental reconstruction algorithm: comparison with echocardiography, SPECT and MR imaging. *Radiology* 2005; 234:381–390
22. Tadamura E, Kudoh T, Motooka M, et al. Assessment of regional and global left ventricular function by reinjection Tl-201 SPECT and rest Tc-99m sestamibi ECG-gated SPECT. *J Am Coll Cardiol* 1999; 33:991–997
23. Tadamura E, Mamede M, Kubo S, et al. The effect of nitroglycerin on myocardial blood flow in various segments characterized by rest-redistribution thallium SPECT. *J Nucl Med* 2003; 44:745–751
24. Cerqueira MD, Weissman NJ, Dilsizian V, et al. Standardized myocardial segmentation and nomenclature for tomographic imaging of the heart: a statement for healthcare professionals from the Cardiac Imaging Committee of the Council on Clinical Cardiology of the American Heart Association. *Circulation* 2002; 105:539–542
25. Tateno S, Terai M, Niwa K, et al. Alleviation of myocardial ischemia after Kawasaki disease by heparin and exercise therapy. *Circulation* 2001; 103:2591–2597
26. Tan LB, Dickie S, McKenna WJ. Left ventricular diastolic characteristics of cardiac sarcoidosis. *Am J Cardiol* 1986; 58:1126–1127
27. Lewin RF, Mor R, Spitzer S, Arditti A, Hellman C, Agmon J. Echocardiographic evaluation of patients with systemic sarcoidosis. *Am Heart J* 1985; 110:116–122
28. Burstow DJ, Tajik AJ, Bailey KR, DeRemee RA, Taliercio CP. Two-dimensional echocardiographic findings in systemic sarcoidosis. *Am J Cardiol* 1989; 63:478–482
29. Bulkley BH, Rouleau JR, Whitaker JQ, Strauss HW, Pitt B. The use of ^{201}thallium for myocardial perfusion imaging in sarcoid heart disease. *Chest* 1977; 72:27–32
30. Kaminaga T, Takeshita T, Yamauchi T, Kawamura H, Yasuda M. The role of iodine-123-labeled 15-(p-iodophenyl)-3R,S-methylpentadecanoic acid scintigraphy in the detection of local myocardial involvement of sarcoidosis. *Int J Cardiol* 2004; 94:99–103
31. Okayama K, Kurata C, Tawarahara K, Wakabayashi Y, Chida K, Sato A. Diagnostic and prognostic value of myocardial scintigraphy with thallium-201 and gallium-67 in cardiac sarcoidosis. *Chest* 1995; 107:330–334
32. Vignaux O, Dhote R, Duboc D, et al. Clinical significance of myocardial magnetic resonance abnormalities in patients with sarcoidosis: a 1-year follow-up study. *Chest* 2002; 122:1895–1901
33. Simonetti OP, Kim RJ, Fieno DS, et al. An improved MR imaging technique for the visualization of myocardial infarction. *Radiology* 2001; 218:215–223
34. Valantine H, McKenna WJ, Nihoyannopoulos P, et al. Sarcoidosis: a pattern of clinical and morphological presentation. *Br Heart J* 1987; 57:256–263
35. Slater GM, Rodriguez ER, Lima JA, Bluemke DA. A unique presentation of cardiac sarcoidosis. *AJR* 2003; 180:1738–1739

Radiology

Masaki Yamamuro, MD
Eiji Tadamura, MD, PhD
Shigeto Kubo, MD, PhD
Hiroshi Toyoda, MD, PhD
Takeshi Nishina, MD, PhD
Muneo Ohba, MD
Ryohei Hosokawa, MD, PhD
Takeshi Kimura, MD, PhD
Nagara Tamaki, MD, PhD
Masashi Komeda, MD, PhD
Toru Kita, MD, PhD
Junji Konishi, MD, PhD

Published online
10.1148/radiol.2342031271
Radiology 2005; 234:381–390

Abbreviations:
ECG = electrocardiographic
EDV = end-diastolic volume
EF = ejection fraction
ESV = end-systolic volume
LV = left ventricle

[1] From the Departments of Nuclear Medicine and Diagnostic Imaging (M.Y., E.T., S.K., H.T., J.K.), Cardiovascular Surgery (T.N., M.K.), and Cardiovascular Medicine (M.O., R.H., T. Kimura, T. Kita), Kyoto University Graduate School of Medicine, 54 Shogoinkawahara, Sakyo-ku, Kyoto 606-8507, Japan; and Department of Nuclear Medicine, Hokkaido University Graduate School of Medicine, Sapporo, Japan (N.T.). Received August 10, 2003; revision requested October 22; final revision received March 20, 2004; accepted May 28. **Address correspondence to** M.Y. (e-mail: *myamamu@kuhp.kyoto-u.ac.jp*).

Authors stated no financial relationship to disclose.

Author contributions:
Guarantor of integrity of entire study, M.Y.; study concepts and design, M.Y.; literature research, M.Y.; clinical studies, E.T., S.K., M.O., R.H., T.N.; experimental studies, M.Y., E.T., S.K., H.T.; data acquisition, E.T., S.K., H.T., M.O., R.H., T.N.; data analysis/interpretation, E.T., S.K., H.T., M.O., R.H.; statistical analysis, M.Y.; manuscript preparation, definition of intellectual content, and editing, M.Y., E.T.; manuscript revision/review, M.O., R.H., T.N., T. Kimura, N.T., M.K., T. Kita, J.K.; manuscript final version approval, all authors

Cardiac Functional Analysis with Multi-Detector Row CT and Segmental Reconstruction Algorithm: Comparison with Echocardiography, SPECT, and MR Imaging[1]

PURPOSE: To evaluate accuracy of cardiac functional analysis with multi-detector row computed tomography (CT) and segmental reconstruction algorithm over a range of heart rates.

MATERIALS AND METHODS: Institutional review board approval was obtained. Informed consent was not required. Multi-detector row CT (500-msec rotation time, 8 × 1-mm detector collimation) and magnetic resonance (MR) imaging were performed in 50 patients (28 men, 22 women; age range, 46–84 years; mean age, 67 years). Two-dimensional echocardiography was performed in 41 patients, and electrocardiographically (ECG)-gated single photon emission computed tomography (SPECT) was performed in 27. End-diastolic volume (EDV), end-systolic volume (ESV), ejection fraction (EF), and left ventricular (LV) mass were estimated with multi-detector row CT and compared with values estimated with MR imaging, which served as the reference standard. Additionally, EF values estimated with multi-detector row CT, echocardiography, and SPECT were compared with those estimated with MR imaging. Systemic error and degree of agreement of global functional parameters measured with MR imaging and other modalities were assessed. In a second analysis, linear regression analysis was added.

RESULTS: EF estimated with multi-detector row CT agreed and correlated well with EF estimated with MR imaging (bias ± standard deviation, −1.2% ± 4.6; r = 0.96). Agreement and correlation were similar for EDV (−0.35 mL ± 15.2; r = 0.97), ESV (1.1 mL ± 8.6; r = 0.99), and LV mass (2.5 mL ± 15.0; r = 0.96). Standard deviation of EF difference between multi-detector row CT and MR imaging was significantly less than that between echocardiography and MR imaging ($P < .001$) or that between SPECT and MR imaging ($P < .001$).

CONCLUSION: Various LV functional parameters were measured with multi-detector row CT with a segmental approach, and measurements correlated and agreed with those obtained with MR imaging. Moreover, functional analysis with multi-detector row CT was more accurate than that with two-dimensional echocardiography or ECG-gated SPECT.

Evaluation of global left ventricular (LV) function, especially ejection fraction (EF), and mass is important in the treatment of various cardiac diseases. To date, cardiac functional assessment has been performed with various noninvasive modalities, such as echocardiography (1,2), nuclear medicine (3), single-detector row helical computed tomography (CT) (4), electron beam CT (5–8), and magnetic resonance (MR) imaging (9–19). Cardiac MR imaging provides excellent temporal and spatial resolution, allows image acquisition

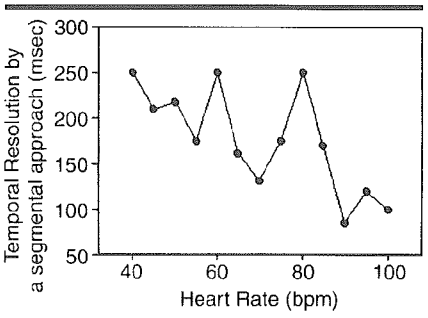

Figure 1. Graph shows temporal resolution of the multi-detector row CT system with segmental approach (rotation time, 500 msec; helical pitch, 2.0) at various heart rates. *bpm* = Beats per minute.

TABLE 1
Patient Characteristics and Final Diagnoses

Characteristics and Diagnoses	Multi-Detector Row CT and MR Imaging	Echocardiography	SPECT
Age (y)*	67 ± 10	67 ± 10	68 ± 10
Sex			
Male	28	22	17
Female	22	19	10
Heart rate (beats per minute)*	71 ± 13	71 ± 13	74 ± 13
Angina pectoris	12	9	12
Myocardial infarction	12	10	11
Valve disease	20	17	1
Other diagnoses	6	5	3
Total diagnoses	50	41	27

Note.—Unless otherwise indicated, data are numbers of patients.
* Data are mean ± standard deviation.

in any desired plane, and has a high degree of accuracy and reproducibility concerning quantitative measurements. In addition, MR imaging can be used to measure LV volume, without assumptions about LV cavity geometry. Thus, MR imaging is currently considered the reference standard in assessment of cardiac function (1,3,9–12,18,19).

In the past few years, multi-detector row CT has been increasingly used for noninvasive coronary artery imaging (20–31). In the evaluation of cardiac function, multi-detector row CT with a temporal resolution of 125–250 msec has been shown to be promising by comparing with biplanar cineventriculography (32) or MR imaging (33). However, it was indicated that reconstructed images obtained in patients with a high heart rate were of low quality because of motion artifacts; thus, manual tracing of endocardial contours had limited accuracy (32,33). A segmental reconstruction algorithm that uses data from several heartbeats has been introduced to further improve temporal resolution (34). The basic principle of segmental reconstruction is that data needed to reconstruct one image are collected retrospectively from several heartbeats by dividing into several segments. Each segment obtained in one cardiac cycle represents a shorter time period. Thus, a segmental reconstruction algorithm is considered to be effective in shortening the temporal resolution and reducing motion artifacts in patients with a high heart rate. Thus, the aim of this study was to evaluate the accuracy of cardiac functional analysis with multi-detector row CT and a segmental reconstruction algorithm over a range of heart rates.

MATERIALS AND METHODS

Phantom Studies

To evaluate artifacts of reconstruction images obtained with two retrospective electrocardiographically (ECG)-gated reconstruction methods, phantom (AZ-631N; Anzai Medical, Tokyo, Japan) studies were performed with various heart rates (every 5% of cardiac cycle, from 40 to 100 beats per minute). Method 1 involved a half reconstruction algorithm, and method 2 involved a segmental reconstruction algorithm that used data from several heartbeats. CT examinations were performed by using a multi-detector row CT scanner with eight detector rows (Aquilion Multi V1.10 JR 002 system; Toshiba, Otawara, Japan). In the scanning protocol, a collimation of 8 × 1 mm, a helical pitch of 2.0, and a rotation time of 500 msec were used. The temporal resolution with a half approach was 250 msec, while the temporal resolution with a segmental approach was further improved, depending on heart rate (Fig 1). Each helical CT scan was obtained with a tube voltage of 135 kV and a tube current of 200 mA. Image reconstruction was performed with a 1-mm increment by using both algorithms for each of these heart rates (35,36). Twenty sets of reconstructions at every 5% of the cardiac cycle, ranging from 0% to 95%, were performed in each study. One short-axis image and two long-axis cine images were reoriented from these sets of reconstruction data by using cardiac MPR software (Toshiba). The optimal end-diastolic and end-systolic phases were visually determined with these cine images.

Artifacts were evaluated on the reconstructed end-diastolic and end-systolic images of the different heart rates by two observers, each with 2 years of experience (S.K. and H.T.). The blurring artifact was scored visually with a five-point scale (0, no artifact; 1, slight artifact; 2, mild artifact; 3, moderate artifact; and 4, severe artifact). The stair-step artifact was scored with a three-point scale (0, no artifact; 1, mild artifact; and 2, severe artifact).

Human Studies

Patients referred for coronary multi-detector row CT from August 2002 to July 2003 for clinical reasons were included in this retrospective study. Among these 50 patients, MR imaging was used to assess cardiac function within 10 days before or after multi-detector row CT, during which time the condition of patients was stable. The study group consisted of 28 men (age range, 47–83 years; mean age, 67 years) and 22 women (age range, 46–84 years; mean age, 67 years). A test for the proportion with normal distribution with a 5% significance level was used to analyze the proportion of men and women, a two-sample *t* test with a 5% significance level was used to analyze the age difference between men and women, and an F test with a 5% significance level was used to analyze equality of variance between the age of men and women. No statistically significant difference was observed regarding age or sex. Mean heart rate during acquisition of CT scans ranged from 49 to 106 beats per minute (mean ± standard deviation, 71 beats per minute ± 13). A total of 20 patients had aortic and/or mitral valve disease, 12 had myocardial infarction, 12 had angina pectoris, two had infectious endocarditis, two had sarcoidosis, one had pericarditis, and one had dilated cardiomyopathy. During the same period, conventional two-dimensional echocardiography was performed in 41 patients, and ECG-gated single photon emission computed tomography (SPECT) was performed in 27. Patient characteristics and final diagnoses are shown in Table 1. Our

TABLE 2
Mean Artifact Scores in End-Diastolic and End-Systolic Phases with Half and Segmental Reconstruction Algorithms

Reconstruction Algorithm and Artifact	Heart Rate (beats/min)												
	40	45	50	55	60	65	70	75	80	85	90	95	100
	End-Diastolic Phase												
Half reconstruction algorithm													
Blurring artifact	0.0	0.0	0.0	0.0	0.5	1.0	1.5	1.0	1.0	1.0	2.0	2.5	3.0
Stair-step artifact	0.0	0.0	0.0	0.0	0.0	1.0	1.5	0.0	0.0	1.0	1.5	1.5	2.0
Segmental reconstruction algorithm													
Blurring artifact	0.0	0.0	0.0	0.0	0.5	0.0	0.0	1.0	1.0	0.0	0.0	0.0	1.0
Stair-step artifact	0.0	0.0	0.0	0.0	0.0	0.0	0.0	0.0	0.0	0.0	0.0	0.0	0.0
	End-Systolic Phase												
Half reconstruction algorithm													
Blurring artifact	0.0	0.5	1.0	1.5	1.5	2.5	2.5	3.0	3.0	3.0	3.5	4.0	4.0
Stair-step artifact	0.0	0.0	0.0	0.0	0.0	1.0	2.0	1.5	0.0	1.0	1.5	2.0	2.0
Segmental reconstruction algorithm													
Blurring artifact	0.0	0.5	1.0	0.5	1.5	1.0	1.5	1.5	3.0	2.0	0.5	1.0	2.0
Stair-step artifact	0.0	0.0	0.0	0.0	0.0	0.0	0.5	0.0	0.0	0.0	0.0	0.0	0.0

institutional review board approved this retrospective study. Informed consent was not required.

Multi–Detector Row CT and Image Interpretation

The CT scanner and scanning protocol used to examine patients were the same as those used in the phantom studies. The estimated effective radiation dose was 7.4 mSv. All patients received 100–150 mL of nonionic contrast agent through an intravenous antecubital catheter infused with a flow rate of 3.0–3.5 mL/sec without any premedication. The scanning delay was set with an automatic triggering system (SureStart; Toshiba) (37). As soon as the signal density level in the ascending aorta, which was monitored in real time, reached a predefined threshold of 150 HU, the patient was automatically instructed to maintain a breath hold; at this time, CT data and an ECG trace were obtained. Both a half and a segmental reconstruction algorithm were also applied in human studies. With the ECG trace, retrospective reconstruction was performed for acquisition of phase images starting from early systole (0% of the R-R interval) and ending at the end of diastole (95% of the R-R interval) by using 5% increasing steps; thus, 20 heart phases were obtained. One short-axis image and two long-axis cine images were created with these reconstructed data by using the same software that was used in phantom experiments. The end-diastolic and end-systolic phases were visually determined with these cine images. Short-axis images of the two phases, which covered the whole heart (10-mm section thickness), were used for functional analysis.

CT images were analyzed by an experienced observer (S.K.) without any clinical information. Manual adjustments of endocardial and epicardial borders of each short-axis image were performed. As previously described, papillary muscles were regarded as being part of the LV cavity (10,18). Subsequently, end-diastolic volume (EDV), end-systolic volume (ESV) (both were measured in milliliters), and LV mass (measured in grams) were calculated on the basis of the Simpson rule. LV mass was calculated as a product of the specific gravity of the myocardium (ie, 1.05 g/cm^3) and integrated LV myocardial area (10). Finally, the percentage of EF was calculated with EDV and ESV data (38).

Interobserver Variability of CT Measurements

Because the repeatability of multi–detector row CT measurements is relevant to the amount of agreement, interobserver variability was tested by comparing measurements obtained by two experienced observers (S.K., H.T.) at different times and without any clinical information by using data sets obtained in the first 20 patients.

MR Imaging and Image Interpretation

MR imaging was performed with a 1.5-T whole-body imager (Symphony; Siemens, Erlangen, Germany), with multiple surface coils connected to phased-array receivers. Breath-hold cine MR imaging was performed with the segmented steady-state free precession sequence (13–15). Imaging parameters were as follows: repetition time msec/echo time msec, 3.6/1.8; flip angle, 70°; seven to 15 lines per segment; matrix, 208 × 256; and field of view, 340 × 340. Cine MR images of 10–12 contiguous sections with 10-mm section thickness were obtained in the short-axis plane, covering the entire LV from the base to the apex, to acquire three-dimensional LV data (18,19).

MR images were analyzed by an observer (E.T., with 10 years of experience) without any clinical information but with the aid of commercially available software (Argus; Siemens). Image analysis was followed with manual correction of the LV border, as with multi–detector row CT. Subsequently, various functional parameters were measured with the same method.

Echocardiography and Image Interpretation

For two-dimensional echocardiography, patients underwent imaging in the left lateral decubitus position by using a commercially available system (Sonos 5500; Hewlett-Packard, Palo Alto, Calif). Images were obtained by an observer (M.O., with 8 years of experience) using a 3.5-MHz transducer in the parasternal (long- and short-axis) and apical (two- and four-chamber views) planes and were saved in cine loop format. EF was calculated by the same observer, who was

blinded to other information obtained with two- and four-chamber images, and who used the previously validated biplanar Simpson rule (1,2,38–41).

ECG-gated SPECT and Image Interpretation

Each patient underwent exercise thallium 201 (^{201}Tl) SPECT, as described previously (18,42). At the peak exercise level, approximately 74 MBq of ^{201}Tl was injected intravenously. Approximately 10 minutes after the termination of exercise, initial SPECT was performed. Approximately 3–4 hours after termination of the initial examination, an additional 37 MBq of ^{201}Tl was injected, and reinjection SPECT was performed. ECG-gated SPECT images were obtained with a dual-head gamma camera (Millennium; GE Medical Systems, Milwaukee, Wis) equipped with low-energy thin section collimation (30 projections over 180°, eight frames per cardiac cycle, 60 seconds per projection). Two energy windows were used (ie, 30% windows centered on the 70- and 167-keV peaks). ECG-gated perfusion SPECT images were prefiltered with Butterworth filter (order, five; voxel size, 7.2 mm; cutoff frequency, 0.40 cycles per pixel) (18). A zoom factor of 1.28 was used. Data were reconstructed by using a filtered back-projection technique with no attenuation or scatter correction. The EF was automatically calculated with reinjection SPECT images by using the Germano algorithm (3,18,19,43).

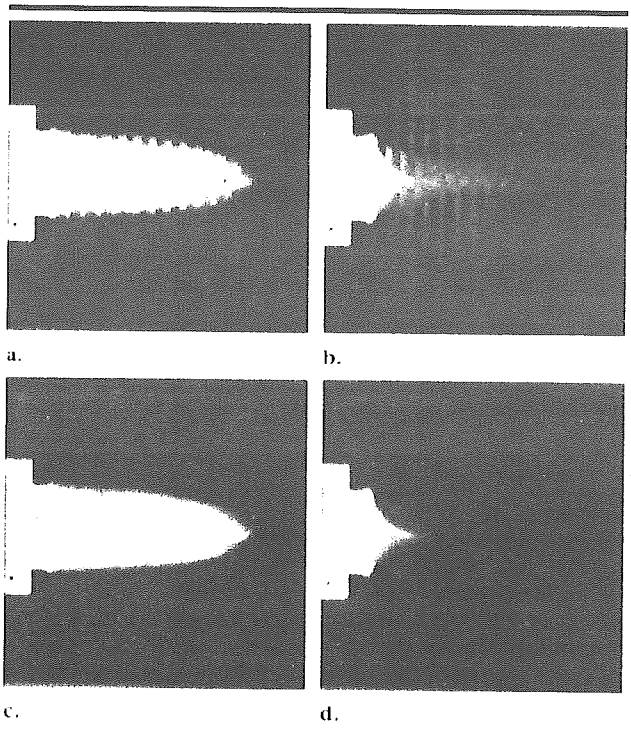

Figure 2. End-diastolic and end-systolic vertical long-axis CT scans of a phantom were reconstructed with half and segmental reconstruction algorithms at a heart rate of 95 beats per minute. **(a)** End-diastolic and **(b)** end-systolic vertical long-axis CT scans obtained with half approach. **(c)** End-diastolic and **(d)** end-systolic vertical long-axis CT scans obtained with segmental approach. Severe artifacts were observed with a half approach, especially in the end-systolic phase, while no severe artifacts were observed with a segmental approach. Artifacts of reconstructed images obtained with a half approach were so severe that determination of the myocardial outline was difficult.

Statistical Analysis

Data are expressed as mean ± standard deviation. Evaluation of agreement between artifact scores of the phantom was performed by using κ statistics. Systemic error and the degree of agreement of global functional parameters obtained with multi–detector row CT and MR imaging were assessed according to the method described by Bland and Altman (44). Systemic error and the degree of agreement of EF, as calculated with echocardiography and MR imaging data and ECG-gated SPECT and MR imaging data, respectively, were assessed with the same method. The degree of agreement between the two methods was determined as the mean difference (bias), standard deviation of the differences, limits of agreement (mean ± 2 standard deviations), standard error of the mean difference, and 95% confidence interval of the mean difference. A one-sample *t* test at the 5% significance level was used to determine whether the resulting difference from zero, as an under- or overestimation with multi–detector row CT, was significant. F ratios were used to describe the equality of the standard deviation of difference of EF values obtained with multi–detector row CT with a segmental reconstruction algorithm and MR imaging to EF values obtained with echocardiography and MR imaging and EF values obtained with ECG-gated SPECT and MR imaging.

In a second analysis, linear regression analysis was used to compare the functional values obtained with multi–detector row CT, echocardiography, and ECG-gated SPECT with MR imaging. F ratios were used to describe the equality of standard error of estimates of EF between the correlation of multi–detector row CT with a segmental reconstruction algorithm and MR imaging, between echocardiography and MR imaging, and between ECG-gated SPECT and MR imaging. A *P* value of less than .05 was considered to indicate statistical significance.

RESULTS

Phantom Studies

The results of phantom studies are shown in Table 2. The κ value for evaluation of agreement between the blurring artifact scores was 0.58, while that between the stair-step artifacts was 0.73. Various artifacts were observed in patients with higher heart rates (≥65 beats per minute) who were evaluated with a half reconstruction algorithm; no substantial artifacts were found in patients evaluated with a segmental reconstruction algorithm, except in those with a heart rate of 80 beats per minute. In patients with higher heart rates (≥65 beats per minute), artifacts of reconstructed images obtained with a half reconstruction algorithm were generally so severe that determination of the myocardial outline was difficult (Fig 2).

Human Studies

No substantial motion artifact was observed, even in patients with a high heart

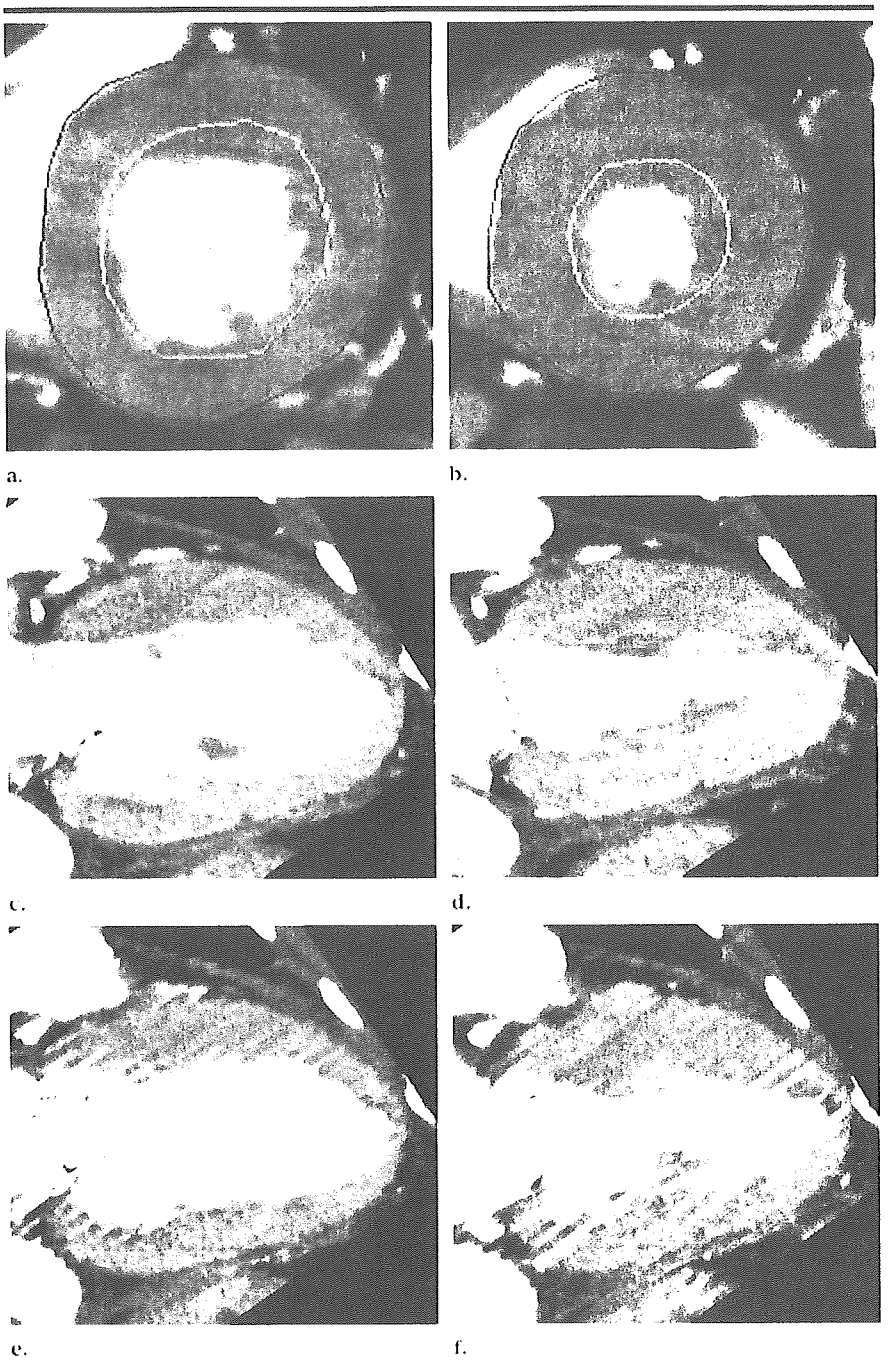

Figure 3. End-diastolic and end-systolic short-axis and vertical long-axis CT scans were reconstructed with a segmental reconstruction algorithm in a patient with a heart rate of 98 beats per minute. (a) Typical end-diastolic and (b) corresponding end-systolic short-axis CT scans. (c) End-diastolic and (d) end-systolic vertical long-axis CT scans. Epicardial (black line in a and b) and endocardial (white line in a and b) tracings exclude epicardial fat and include papillary muscles within ventricular cavity. No severe artifact was found on these scans. End-diastolic and end-systolic vertical long-axis scans were also reconstructed with a half reconstruction algorithm in the same patient. (e) End-diastolic and (f) end-systolic vertical long-axis CT scans. Artifacts of reconstructed images obtained with a half reconstruction algorithm were more severe than those obtained with a segmental approach. Of note, the end systolic size of the LV cavity appeared larger on scans obtained with a half approach than on scans obtained with a segmental approach. Angina pectoris was diagnosed in this patient.

rate, when a segmental reconstruction approach was used. On the other hand, artifacts were generally more severe on reconstructed images obtained with a half approach than on images obtained with a segmental approach if the heart rate was higher (Fig 3).

A summary of data obtained with multi-detector row CT, echocardiography, ECG-gated SPECT, and MR imaging is presented in Tables 3–5. Results of the Bland-Altman analysis are shown in Tables 6–8 and Figures 4–6. Bland-Altman analysis revealed no significant degree of directional measurement bias when data obtained with multi-detector row CT and segmental reconstruction algorithm were compared with data obtained with MR imaging ($n = 50$). No significant difference of the mean difference from 0 was found for any parameter ($n = 50$). On the other hand, significant overestimation of ESV ($P < .01$) and underestimation of EF ($P < .001$) were observed with a half approach ($n = 50$). In terms of EF, the standard deviation of difference between multi-detector row CT with a segmental reconstruction algorithm and MR imaging was significantly less than that between echocardiography and MR imaging ($n = 41$, $P < .001$) or that between ECG-gated SPECT and MR imaging ($n = 27$, $P < .001$).

The results of linear regression analysis are shown in Tables 9–11. The data (EF, EDV, ESV, and LV mass) obtained with multi-detector row CT were closely correlated with the data obtained with MR imaging ($n = 50$). In terms of EF, the standard error of the estimate between multi-detector row CT with a segmental reconstruction algorithm and MR imaging was significantly smaller than that between echocardiography and MR imaging ($n = 41$, $P < .001$) or that between ECG-gated SPECT and MR imaging ($n = 27$, $P < .001$).

Interobserver Variability of CT Measurements

An interobserver variability of 8.6% for EF, 7.3% for EDV, 9.6% for ESV, and 10.4% for LV mass was found with the half reconstruction algorithm. On the other hand, an interobserver variability of 5.7% for EF, 6.9% for EDV, 7.0% for ESV, and 9.3% for LV mass was found with the segmental reconstruction algorithm. These results revealed small interobserver variability among the multi-detector row CT measurements.

DISCUSSION

Our results demonstrate that the LV values, including EF, EDV, ESV, and LV mass, obtained with multi-detector row

TABLE 3
LV Measurements with Multi-Detector Row CT and MR Imaging in 50 Patients

Modality and Algorithm	LV EF (%)	EDV (mL)	ESV (mL)	LV Mass (g)
Multi-detector row CT				
Half reconstruction algorithm	46.5 ± 14.4 (12–70)	153.5 ± 59.4 (81–342)	86.2 ± 53.7 (31–263)	142.2 ± 61.7 (60–347)
Segmental reconstruction algorithm	50.1 ± 16.2 (12–76)	153.7 ± 59.5 (85–322)	81.7 ± 55.8 (27–262)	141.1 ± 56.9 (76–326)
MR imaging	51.3 ± 16.1 (12–78)	154.0 ± 64.3 (63–334)	80.6 ± 57.8 (25–257)	138.6 ± 53.9 (67–316)

Note.—Data are mean ± standard deviation. Data in parentheses are the range.

TABLE 4
LV EF in 41 Patients

Modality	LV EF (%)
Echocardiography	54.6 ± 16.7 (15–86)
Multi-detector row CT with segmental reconstruction algorithm	50.7 ± 16.0 (12–76)
MR imaging	51.8 ± 15.9 (12–78)

Note.—Data are mean ± standard deviation. Data in parentheses are the range.

TABLE 5
LV EF in 27 Patients

Modality	LV EF (%)
ECG-gated SPECT	39.6 ± 17.5 (12–74)
Multi-detector row CT	43.1 ± 15.9 (12–75)
MR imaging	43.3 ± 15.0 (12–67)

Note.—Data are mean ± standard deviation. Data in parentheses are the range.

TABLE 6
Multi-Detector Row CT and MR Imaging in 50 Patients

Algorithm and Statistics	LV EF (%)	EDV (mL)	ESV (mL)	LV Mass (g)
Half reconstruction algorithm				
Bias*	−4.7 ± 6.0	−0.49 ± 18.2	5.5 ± 12.4	3.6 ± 19.9
Limits of agreement†	12.0	36.3	24.8	39.8
95% CI	1.7	5.0	3.4	5.5
Standard error of the mean difference	0.8	2.6	1.8	2.8
Regression line	$y = -0.11 \times +0.8$	$y = -0.08 \times +12.1$	$y = 0.075 \times +11.8$	$y = 0.14 \times -16.0$
Segmental reconstruction algorithm				
Bias*	−1.2 ± 4.6	−0.35 ± 15.2	1.1 ± 8.6	2.5 ± 15.0
Limits of agreement†	9.3	30.5	17.3	30.0
95% CI	1.3	4.2	2.4	4.2
Standard error of the mean difference	0.7	2.2	1.2	2.1
Regression line	$y = 0.005 \times -1.5$	$y = -0.079 \times +11.7$	$y = -0.036 \times +4.0$	$y = 0.057 \times -5.4$

Note.—Bland-Altman analysis revealed significant overestimation of ESV ($P < .01$) and underestimation of EF ($P < .001$) in a half approach compared with MR imaging. No significant degree of directional measurement bias was observed in any of the comparisons of multi-detector row CT with a segmental reconstruction algorithm and MR imaging data. No significant difference of the mean difference from 0 was found for any parameter with a segmental approach. CI = confidence interval.
* Data are mean ± standard deviation.
† Two standard deviations.

CT and a segmental reconstruction algorithm correlated and agreed with those obtained with MR imaging over a wide range of heart rates. Moreover, functional analysis with multi-detector row CT and a segmental reconstruction algorithm was more accurate than analysis performed with two-dimensional echocardiography or ECG-gated SPECT.

Among the many factors that may affect the accuracy of LV functional measurements with multi-detector row CT, the main limitation is the fact that temporal resolution is worse with multi-detector row CT than with MR imaging (ap-

TABLE 7
EF Difference between Multi-Detector Row CT and MR Imaging and between Echocardiography and MR Imaging

Statistics	Multi-Detector Row CT and MR Imaging (%)	Echocardiography and MR Imaging (%)
Bias*	−1.1 ± 4.1	2.6 ± 9.3
Limits of agreement†	8.2	18.6
95% CI	1.3	2.9
Standard error of the mean difference	0.6	1.5
Regression line	$y = 0.007 \times -1.5$	$y = 0.41 \times +0.38$

Note.—The standard deviation of difference between multi-detector row CT and MR imaging was significantly less than that between echocardiography and MR imaging ($P < .001$). CI = confidence interval.
* Data are mean ± standard deviation.
† Two standard deviations.

TABLE 8
EF Difference between Multi-Detector Row CT and MR Imaging and between ECG-gated SPECT and MR Imaging

Statistics	Multi-Detector Row CT and MR Imaging (%)	ECG-gated SPECT and MR Imaging (%)
Bias*	−0.2 ± 3.7	−3.6 ± 9.9
Limits of agreement†	7.4	19.8
95% CI	1.4	3.7
Standard error of the mean difference	0.7	1.9
Regression line	y = 0.062 × −2.8	y = 0.17 × −10.8

Note.—The standard deviation of difference between multi-detector row CT and MR imaging was significantly less than that between ECG-gated SPECT and MR imaging ($P < .001$). CI = confidence interval.
* Data are mean ± standard deviation.
† Two standard deviations.

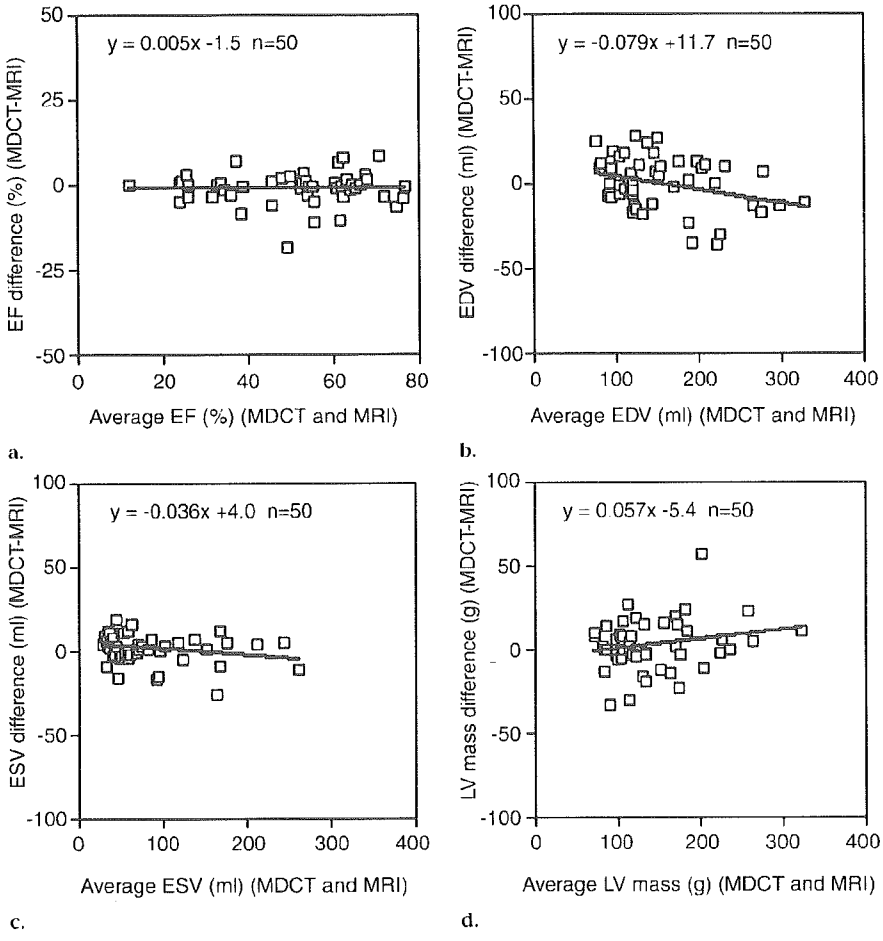

Figure 4. Graphs created with Bland-Altman analysis of (a) LV EF, (b) EDV, (c) ESV, and (d) LV mass, as measured with multi-detector row CT *(MDCT)* with a segmental reconstruction algorithm and MR imaging in 50 patients. Graphs show close agreement between multi-detector row CT and MR imaging. The slopes of the regression lines were not significantly different from 0. No significant differences of the mean difference from 0 were found.

proximately 50 msec). A single helical CT study with a temporal resolution of 400 msec (4) and recent multi-detector row CT studies with a temporal resolution of 125–250 msec performed with a half or biphasic reconstruction algorithm showed close correlation with cineventriculography (32) and MR imaging (33) studies, in terms of EF. Because of the limited temporal resolution, however, systolic images, especially those obtained in patients with a higher heart rate, were shown to be of lower quality (32,33). Additionally, ESV was overestimated, while EDV was not significantly different (4). As a result, underestimation of EF was noted in these studies. In our study, artifacts of reconstructed images obtained with a half approach (temporal resolution of 250 msec) were generally severe if the heart rate was high. In addition, overestimation of ESV and underestimation of EF were observed when a half approach was applied. Juergens et al (32) suggested that data reconstruction algorithms that use segmental data from several heartbeats will likely allow optimization of the analysis of cardiac function with multi-detector row CT. In fact, our phantom experiments demonstrated that a segmental reconstruction algorithm, in which several sets of heartbeat data were used, was more appropriate than a half reconstruction algorithm in terms of reducing motion artifacts, especially in patients with high heart rates.

In the current human studies, no substantial motion artifact was observed, even in patients with a high heart rate, when a segmental reconstruction approach was used. In addition, the various LV functional values obtained with multi-detector row CT and a segmental reconstruction method were shown to correlate and agree with those obtained with MR imaging, which was in agreement with the findings of the preliminary study of Halliburton et al (34). Of note, the standard deviation of EF difference between multi-detector row CT with a segmental approach and MR imaging was significantly less than that between echocardiography and MR imaging or ECG-gated SPECT and MR imaging. Thus, functional analysis with multi-detector row CT and a segmental approach was considered more accurate than functional analysis with two-dimensional echocardiography or ECG-gated SPECT. Previous reports (1,2) suggest that two-dimensional echocardiography is a poor modality to use in the assessment of LV volume and function when ventricular geometry is not uniform. ECG-gated SPECT is also limited when large LV perfusion defects exist (45) or the heart is small (46).

In general, a segmental reconstruction algorithm is effective in shortening the temporal resolution and reducing motion artifacts. At a certain heart rate, however, temporal resolution is not improved, even with a segmental reconstruction approach.